Chapter 8

Results and Discussion

In this chapter we present results for the resonance parameters of the η_c and χ_2 resonances, as well as the results of searches for η_c' and χ_0. The data, which were collected at 146 energy points, spanning $\sqrt{s} = 2911$ MeV to 4289 MeV, have been selected according to the criteria presented in Chapter 7.

We present the cross sections for the reaction $\bar{p}p \to \gamma\gamma$ for both $|\cos\theta^*| \leq 0.2$ and $|\cos\theta^*| \leq 0.4$ in Figs. 8.1- 8.3. For clarity, data points taken at similar energies have been summed. All analyses are performed on the raw, unsummed data, however. The number of $\gamma\gamma$ candidates events, luminosity, total efficiency and cross section for each data point are tabulated in Appendix E, for each of the two choices of $|\cos\theta^*|$ cut.

These data show clear enhancements at ~ 2985 and ~ 3556 MeV, corresponding to η_c and χ_2, respectively, and a suggestion of enhancement at ~ 3415 MeV, corresponding to χ_0. No clear enhancement is discernible in the region in which η_c'

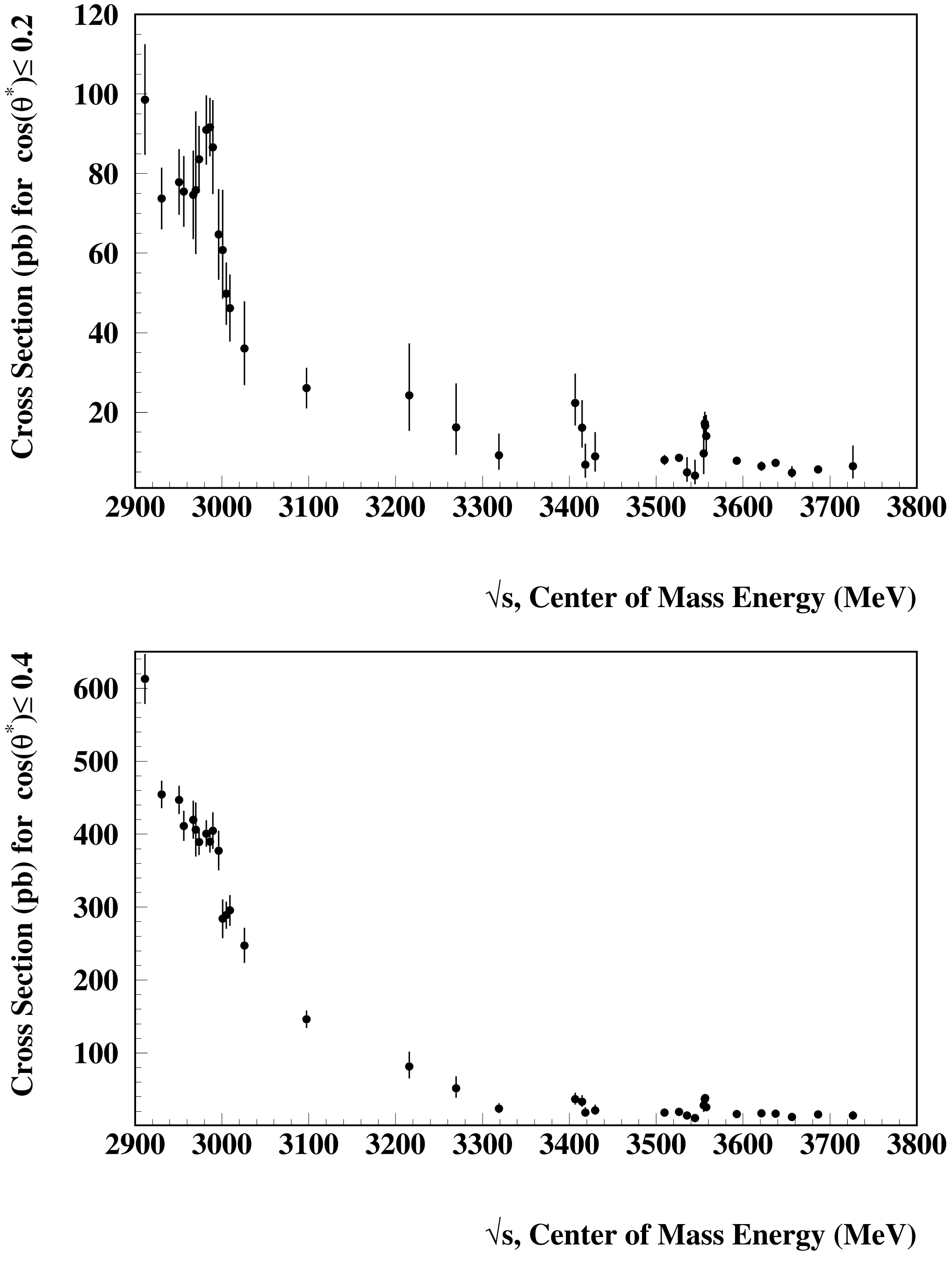

Figure 8.1: $\gamma\gamma$ Cross Sections for (top) $|\cos\theta^*| \leq 0.2$ and (bottom) $|\cos\theta^*| \leq 0.4$.

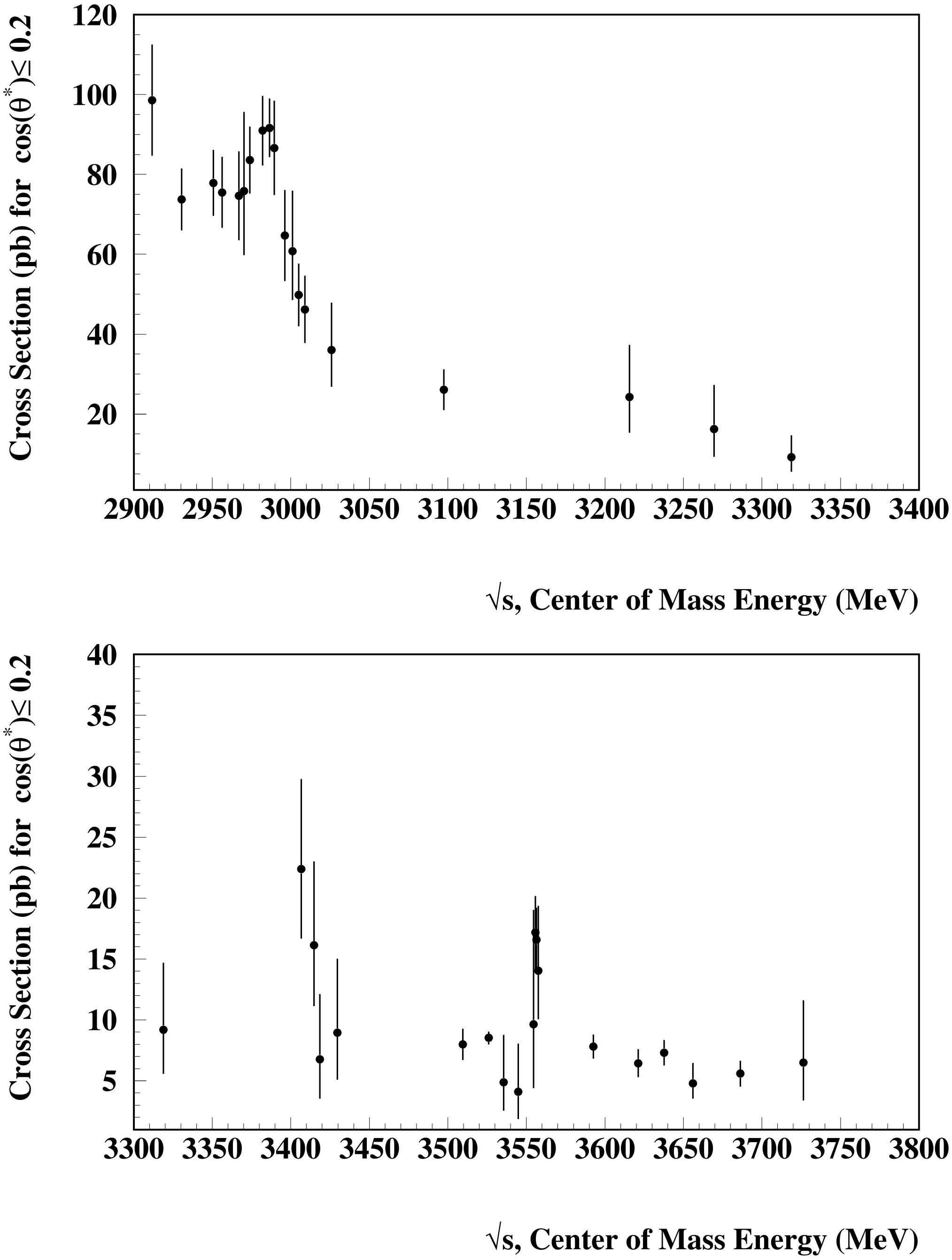

Figure 8.2: $\gamma\gamma$ Cross Sections for $|\cos\theta^*| \leq 0.2$, for CM energies (top) 2900-3400 MeV and (bottom) 3300-3800 MeV.

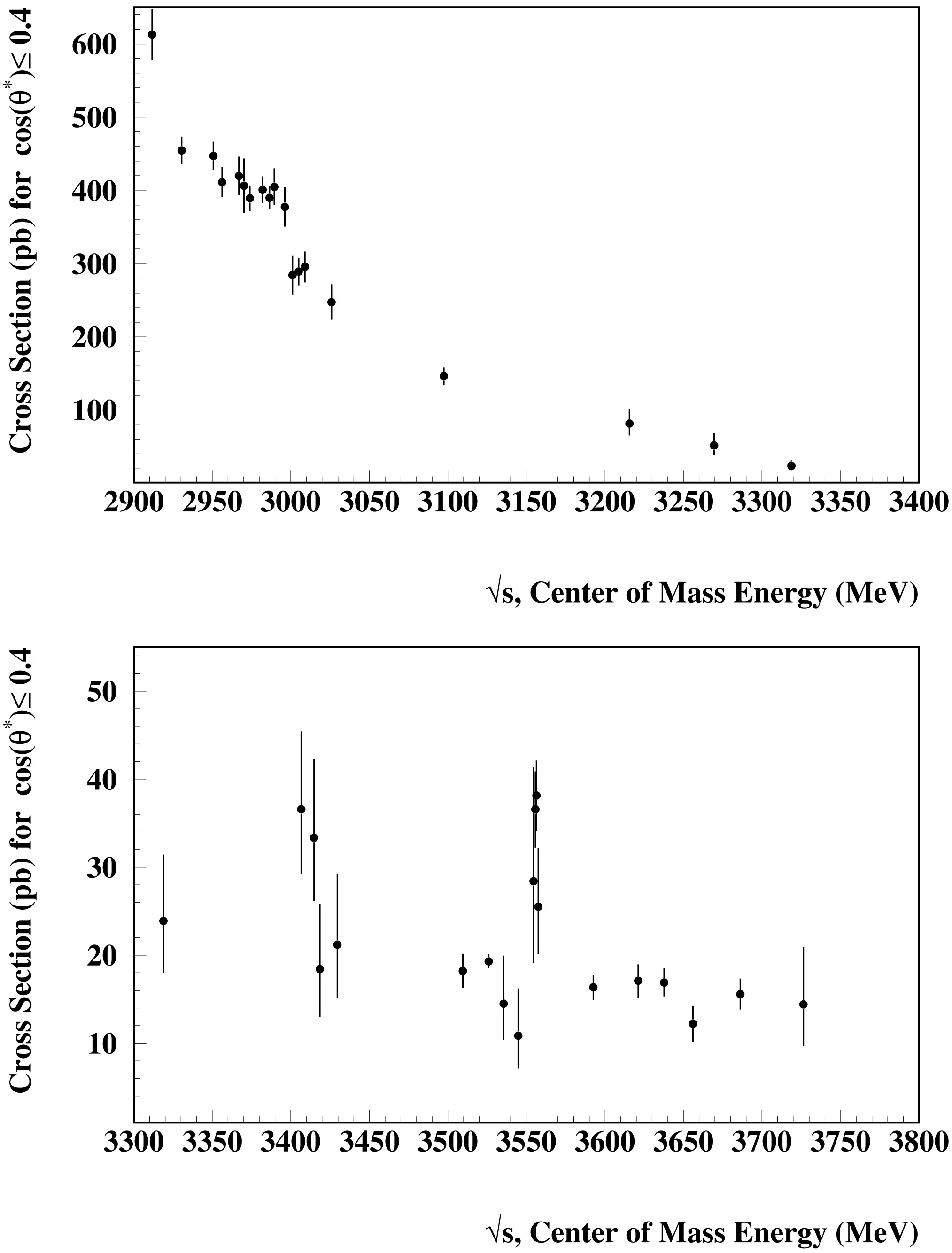

Figure 8.3: $\gamma\gamma$ Cross Sections for $|\cos\theta^*| \leq 0.4$, for CM energies (top) 2900-3400 MeV and (bottom) 3300-3800 MeV.

is expected ($\sim 3600 - 3650$ MeV). These figures demonstrate that even at the η_c resonance, which is clearly visible, a significant amount of background remains.

8.1 Background contributions to $(c\bar{c})_R \to \gamma\gamma$

There has been much speculation as to the source of the backgrounds in the detection of the $\gamma\gamma$ final state in E760 and E835. As mentioned in Chapter 7, the majority of the background is thought to be due to $\pi^0\gamma$ and $\pi^0\pi^0$ events in which one or two photons, respectively, are undetected, and the events thus appear in the CCAL as a single pair of γs.

The E760 Approach to the Background Problem

E760 studied the sensitivity of the η_c resonance parameters to several assumptions about the nature of the background. In all cases, the mass of η_c was found to be stable at ~ 2989 MeV. The total width of the resonance, $\Gamma(\eta_c)$, was found to vary between 17 and 31 MeV, and the product $B(\eta_c \to \bar{p}p) \times \Gamma(\eta_c \to \gamma\gamma)$ was found to vary between 7.7 and 9.2 keV depending on different choices of $|\cos\theta|_{max}$ and different assumptions about the background. In the following we review the E760 approach in order to decide whether or not to use the same method of analysis for the present data.

In E760, the background contributions to the $\gamma\gamma$ final state were estimated by means of a Monte Carlo calculation of the fraction of the measured $\pi^0\pi^0$ and $\pi^0\gamma$ cross sections which feed down into, or fake, the $\gamma\gamma$ channel. The resulting calcu-

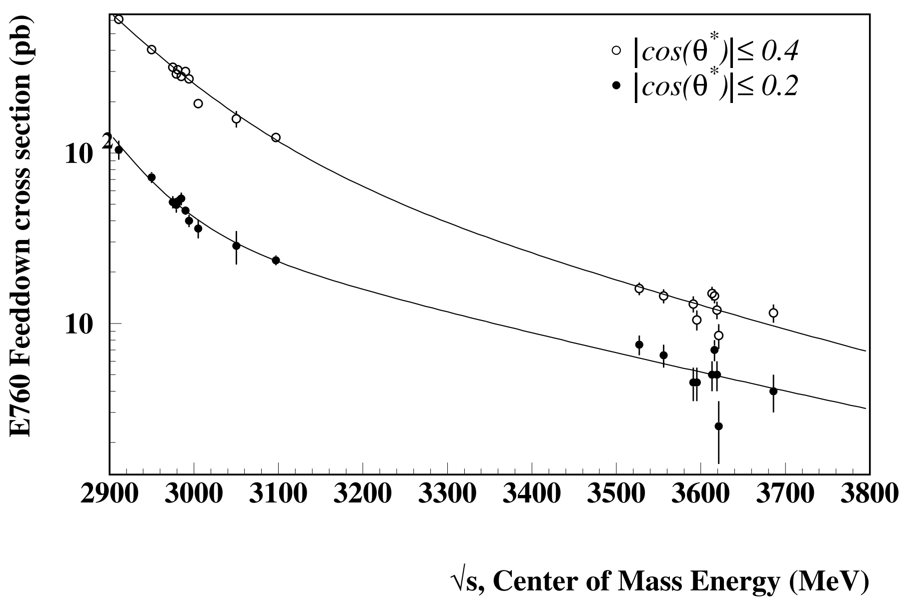

Figure 8.4: Calculated feed-down cross sections based on E760 measurements. The cross sections are calculated by multiplying the measured $\pi^0\pi^0$ and $\pi^0\gamma$ cross sections by the Monte Carlo generated fraction of such events which feed into the $\gamma\gamma$ channel. The data have been taken from Ref. [51]. The functions are the results of fits to the form of Eq. 8.7, which we have used to fit the E835 background to $\gamma\gamma$.

lated "feed-down" cross sections (shown in Fig. 8.4) were treated as data, with the statistical errors assumed to be the small errors in the $\pi^0\pi^0$ and $\pi^0\gamma$ measured cross sections. These calculated cross sections were $\sim$ 50 pb and $\sim$ 300 pb under the η_c peak for $|\cos\theta^*| \leq 0.2$ and $|\cos\theta^*| \leq 0.4$, respectively, and $\sim$ 13.6 pb under the χ_2 peak for $|\cos\theta^*| \leq 0.4$.

The calculated feed-down cross sections, along with the observed $\gamma\gamma$ cross sections, were then fitted in two different regions (2900-3100 MeV for η_c, and 3524-3686

MeV for η_c') separately. * The cross sections were fitted to background functions of the form $A \times (\sqrt{s_0}/\sqrt{s})^B$ plus the Breit-Wigner resonance functions. The implicit assumption in this procedure was that the feed-down calculations predicted the background accurately and completely, and that the continuum cross section $\bar{p}p \rightarrow \gamma\gamma$ was negligibly small.

E760 did, however, make an attempt to estimate possible continuum cross sections $\sigma(\bar{p}p \rightarrow \gamma\gamma)$ allowed by their data and the feed-down calculations. They concluded that 90% confidence upper limits could be set for the continuum cross sections of 21.6 pb for $|\cos\theta^*| \leq 0.25$ at $\sqrt{s} = 2988$ MeV, and 2.3 pb for $|\cos\theta^*| \leq 0.4$ at $\sqrt{s} = 3600$ MeV.

Experimental data for the inverse reaction, $\gamma\gamma \rightarrow \bar{p}p$ exist for CM energies below 3.1 GeV. The two latest measurements are those reported by CLEO [55] and VENUS [54]. These are presented in Fig. 8.5. Although the statistics of both measurements are poor in the vicinity of 3.0 GeV, no enhancement in the measured cross sections is seen in the η_c vicinity, and we can safely conclude that the cross sections represent the continuum yield.

The two measurements give consistent results. At 3.0 GeV, both experiments report $\sigma(\gamma\gamma \rightarrow \bar{p}p) \approx 140$ pb integrated over the region $|\cos\theta^*| \leq 0.6$. Both also give enough angular distribution data to lead to the estimate that $\sigma(|\cos\theta^*| \leq 0.2)$ is $\sim 20\%$ of $\sigma(|\cos\theta^*| \leq 0.6)$. (see Fig. 8.6) From this we conclude that $\sigma(\gamma\gamma \rightarrow \bar{p}p, |\cos\theta^*| \leq 0.2) = 28$ pb, with an estimated error of $\leq 50\%$. In Ref. [56],

*The analysis of the $\chi_2 \rightarrow \gamma\gamma$ reaction in E760 was done before the feed-down technique was developed. In this analysis, the background was *assumed* to have the shape $A \times (\sqrt{s_0}/\sqrt{s})^B$, but no attempt was made to calculate the background level from the possible background processes.

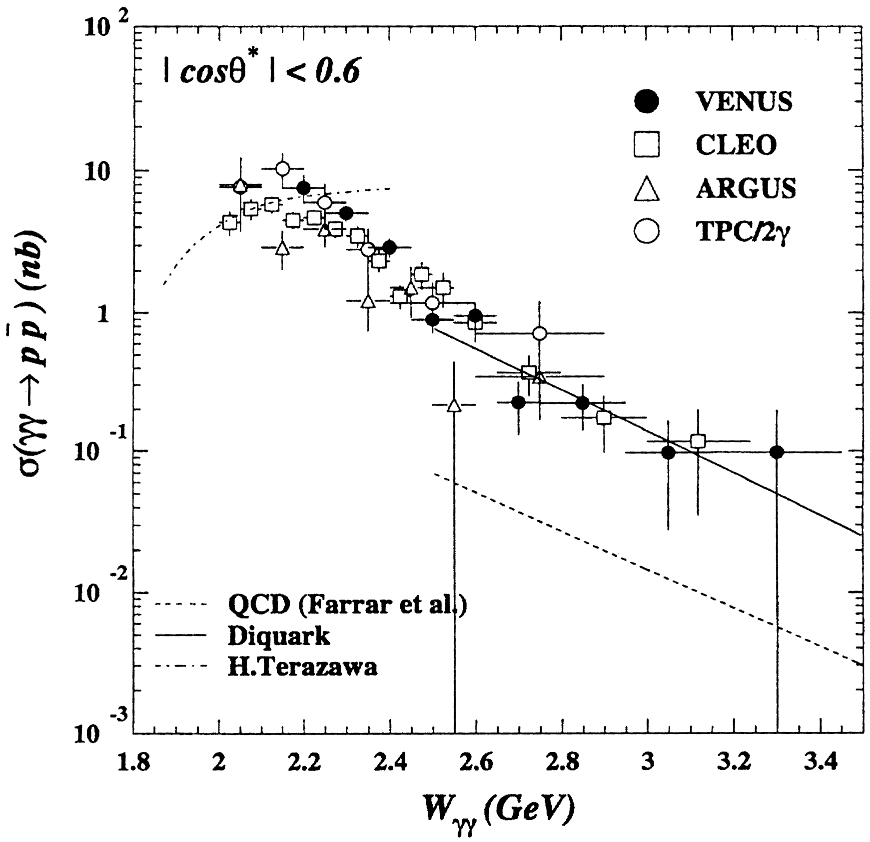

Figure 8.5: Measured cross sections for the reaction $\gamma\gamma \to \bar{p}p$ for $|\cos\theta^*| \leq 0.6$, as a function of CM energy. [54]

Kroll states that $\sigma(|\cos\theta^*| \leq 0.2) = 34$ pb. In the calculations which follow, we will use our slightly lower estimate.

We can estimate a continuum cross section for $\bar{p}p \to \gamma\gamma$ from the above measurement of $\sigma(\gamma\gamma \to \bar{p}p)$ by CLEO and VENUS by using the principle of detailed balance. In general, for a two-body reaction $a + b \to c + d$, the cross section is

$$\sigma(ab \to cd) \propto (2s_c + 1)(2s_d + 1) \times p_{c,d}^2 \times |\mathcal{M}_{ab \to cd}|^2, \tag{8.1}$$

where s_c and s_d are the spins of the final state particles, $p_{c,d}$ the momentum of one of the final state particles in the center of mass frame, and $\mathcal{M}_{ab \to cd}$ is the matrix element for the process. The principle of detailed balance states that the matrix elements for the two inverse processes are the same, *i.e.* that $\mathcal{M}_{ab \to cd} = \mathcal{M}_{cd \to ab}$. Thus, we can relate the cross sections for the reaction $a + b \to c + d$ to that for the reaction $c + d \to a + b$ by the following:

$$\sigma(ab \to cd) = \frac{(2s_c + 1)(2s_d + 1)}{(2s_a + 1)(2s_b + 1)} \times \frac{p_{c,d}^2}{p_{a,b}^2} \times \sigma(cd \to ab). \tag{8.2}$$

We will now apply the results of Eq. 8.2 to the problem at hand.

At $\sqrt{s} = 3.0$ GeV, the center of mass momentum of the $\bar{p}$ is equal to $p(\bar{p}) = \sqrt{s/4 - m^2(\bar{p})} = 1.17$ GeV. The center of mass momentum of the γ is simply 1.5 GeV, therefore the momentum factor $(p_{c,d}^2/p_{a,b}^2) = 1.64$.

The products of spin factors $(2s_1+1)(2s_2+1)$ require some careful consideration. While it is obvious that the proton and antiproton, being fermions with spin s=1/2, each have spin factors $(2s + 1) = 2$, the photon spin factor is not $(2s + 1) = 3$ as one might think, considering that the photon spin is 1.

In the reaction $\bar{p}p \to \gamma\gamma$, two *real* photons are produced. Real photons can have

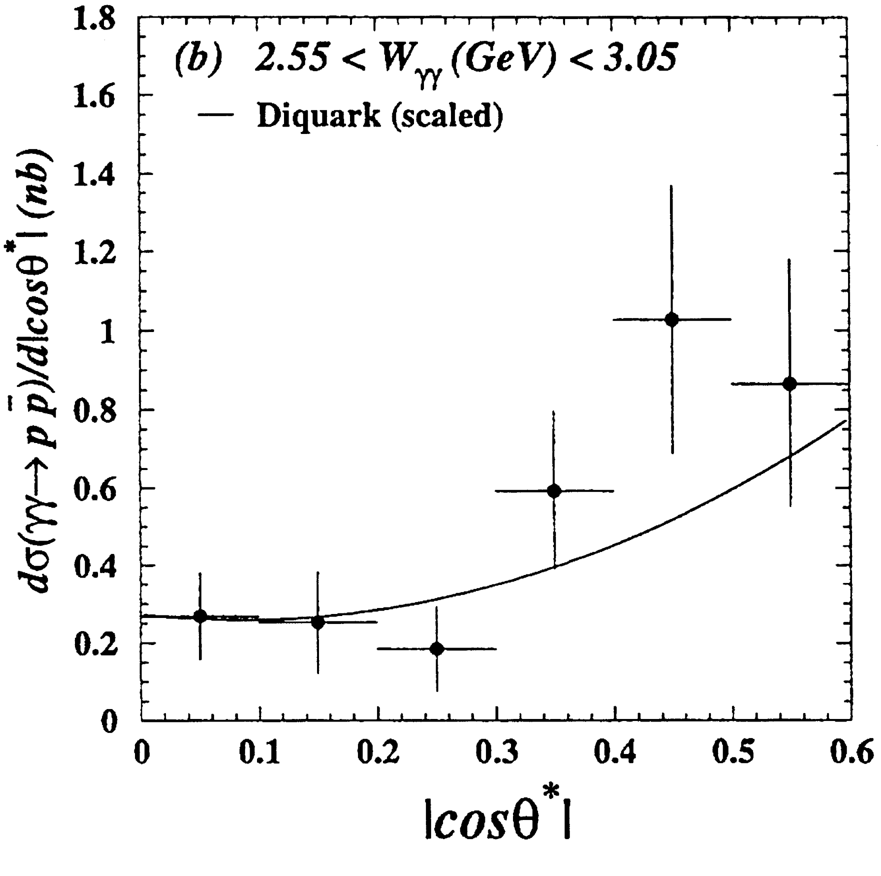

Figure 8.6: Measured differential cross section for the reaction $\gamma\gamma \to \bar{p}p$ from VENUS, for CM energies $2.55 < W < 3.05$ GeV. [54]

only helicities +1 or -1, *i.e.*, the z component of their spins can only be ± 1. Consequently, the factors (2s+1) for the photons must be replaced by 2, and not 3.

Therefore, at $\sqrt{s} = 3.0$ GeV,

$$\sigma(\bar{p}p \rightarrow \gamma\gamma) = 1.64 \times \sigma(\gamma\gamma \rightarrow \bar{p}p). \tag{8.3}$$

Thus, we estimate the continuum cross section for $\bar{p}p \rightarrow \gamma\gamma$ at $\sqrt{s} = 3.0$ GeV, integrated over $|\cos\theta^*| \leq 0.2$, to be 28 pb $\times 1.64 \simeq 46 \pm \leq 23$ pb.

This measured continuum cross section contribution of $46 \pm \leq 23$ pb at $\sqrt{s} =$ 3000 MeV is large enough for us to question the reliability of the E760 results which do not take this into account. It is indeed instructive to find out how much the E760 results would change if a continuum cross section contribution were added to the background estimate based on the feed-down calculations alone. We have tried to estimate this change by fitting the E760 data with the feed-down background alone, and also with the feed-down background increased (very conservatively) by just 30% of the CLEO/VENUS contribution, *i.e.*, by 14 pb at the resonance energy, and having the same functional form as the feed-down background. The two fits are shown in Fig. 8.7. It is found that the resonance mass remains unchanged, but the total and partial widths change substantially. The results are:

Feed-down background (FB) only (same as in Ref. [50]):

$$\Gamma(\eta_c) = 23.8^{+12.8}_{-7.0} \text{ MeV} , \quad \Gamma(\eta_c \rightarrow \gamma\gamma) = 6.6^{+3.9}_{-2.4} \text{ keV} \tag{8.4}$$

FB + 0.3 $\times$ measured continuum contribution:

$$\Gamma(\eta_c) = 19.0^{+11.5}_{-6.5} \text{ MeV} , \quad \Gamma(\eta_c \rightarrow \gamma\gamma) = 4.3^{+2.9}_{-1.9} \text{ keV}. \tag{8.5}$$

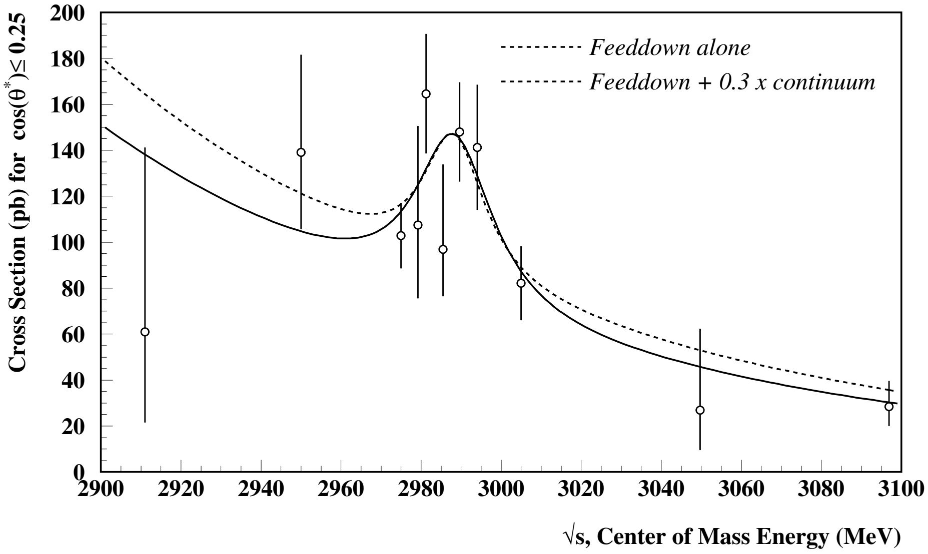

Figure 8.7: Results of two fits to the E760 $\gamma\gamma$ cross sections. The solid line represents the result of a fit to the η_c Breit-Wigner and the calculated feed-down background alone, while the dashed line represents the result of a fit to the η_c Breit-Wigner and the feed-down background plus 30% of the continuum cross sections estimated from the CLEO/VENUS measurements of $\sigma(\gamma\gamma\rightarrow\bar{p}p)$.

This exercise tells us that while we may not have an exact measure of the continuum cross section and/or its variation with $\sqrt{s}$, it is rather dangerous to rely on the calculated feed-down cross sections as a measure of the total background. It is far more prudent to not make any *a priori* assumptions about the background, and to let the data place it wherever it does in a fit in which all parameters are free.

Present Approach to the Background Problem

In view of the above discussion about the perils of using feed-down calculation estimates as measures of the true background, we have investigated several alternative approaches to the background problem.

The first point to settle is about the functional form to be assigned to the background variation with $\sqrt{s}$. E760 claimed to determine the background 'shape' via a fit to the high statistics feed-down cross sections. The functional form

$$\sigma_{bkg} = A \times \left(\frac{\sqrt{s_0}}{\sqrt{s}} \right)^B \tag{8.6}$$

was found to fit the data rather well in the small, *separate* energy regions, $2900 \leq \sqrt{s}(\text{MeV}) \leq 3100$ for η_c and $3524 \leq \sqrt{s}(\text{MeV}) \leq 3686$ for η_c'. No attempt was made to find a single functional form for the entire energy region $2900 \leq \sqrt{s}(\text{MeV}) \leq 3686$. Our situation is different in two respects.

First, since we have chosen not to use high statistics cross sections from a feed-down calculation, we have at our disposal only the measured cross sections with their unflattering statistical errors. These errors are reasonably small in the χ_2, η_c' region, $3500 \leq \sqrt{s}(\text{MeV}) \leq 3800$ MeV, but are quite large in the η_c region, particularly below the resonance.

Second, since we have data, more or less continuously, in the entire energy region $2900 \leq \sqrt{s}(\text{MeV}) \leq 3800$ MeV, we feel that a single functional fit should be obtained for this entire region. This is not easy to begin with, but is rendered more difficult because of the great disparity between the statistical precision of the data in the low energy region, $\sqrt{s} \leq 3400$ MeV, and in the high energy region, $\sqrt{s} \geq 3400$ MeV. As a result, a χ^2 or maximum likelihood fit tends to, in effect, decouple the two regions,

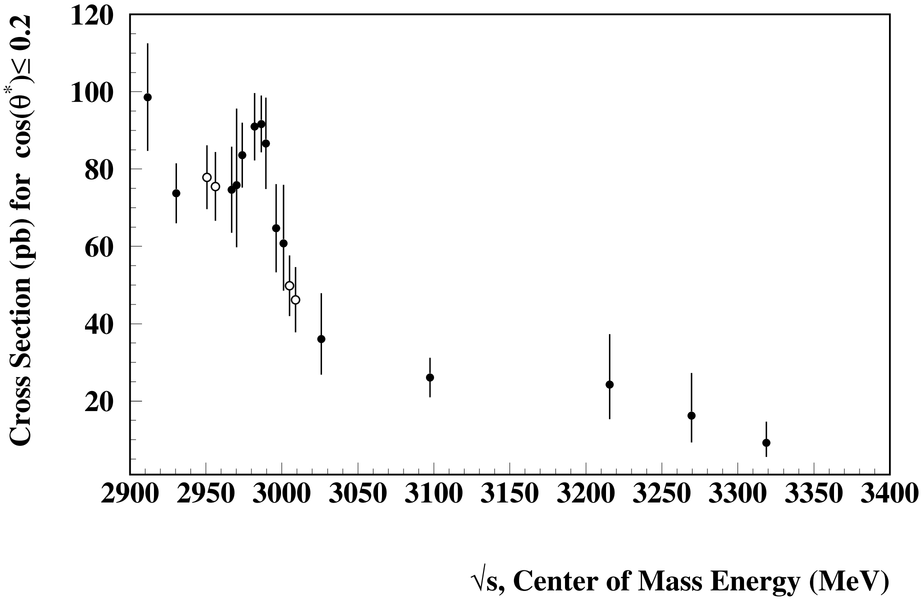

Figure 8.8: $\gamma\gamma$ Cross Sections for $|\cos\theta^*| \leq 0.2$, for CM energies from 2900 to 3400 MeV. The data points represented by the open circles are those which we have considered either "background" or "resonance" points in our attempt to determine the form of the background.

with large uncertainty in the parameters which control the low energy region, and much smaller errors in the parameters which control the high energy region.

We have tried several functional forms to fit the variation of the background with $\sqrt{s}$. All such attempts suffer from the problems caused by the lack of statistical precision in the low energy cross sections, and from how we define the 'background' region in the vicinity of the η_c resonance. We describe the results of our investigations below.

After much searching, the best functional form we have determined is

$$A \times \left(\frac{2985}{\sqrt{s}}\right)^{B} + C \times \left(\frac{3556}{\sqrt{s}}\right)^{D}. \tag{8.7}$$

As we mentioned above, it is important to specify which of the data points should be considered "resonance" points, and which should be considered "background" points. The choice is crucial, especially if the number of "background" points is small. In Fig. 8.8, which shows the data in the η_c region, it is clear that the points at 3025 MeV or above, and at $\sim$ 2930 MeV or below, are far enough away from η_c to be considered background. The data points at 2950 and 2956 MeV, and 3004 and 3009 MeV, indicated by the open circles, could conceivably be considered either background or resonance points. This ambiguity gives rise to a large variation of the background determination, depending on which of the points we include in the background fit.

We have studied this variation by fitting the data to Eq. 8.7, always excluding the χ_0, χ_2 and η_c' points, and those between 2960 and 3001 MeV. In each fit, we also excluded some, or all, of the four points mentioned above. A summary of the results of this study is shown in Table 8.1. The background functions resulting from the different fits are presented in Fig. 8.9. These results show that the parameters C and D, which determine the fit in the high energy region, remain stable because of the good statistical precision of the data in that region. However, the parameters A and B vary by large amounts, leading to up to $\sim$ 10 pb variation in the level of the background at $\sim$ 2988 MeV. This investigation makes it clear that because of our poor statistics we cannot make an independent determination of the background. We have therefore chosen to fit the entireity of our data, including both the resonance

Table 8.1: Summary of results of fitting the background curve (Eq. 8.7) to the data for $|\cos\theta^*| \leq 0.2$. Each line in the table indicates the results of a fit in which only the data points marked by ($\surd$) are included. Other points, indicated by ($-$), are omitted.

	Energy points				Background Parameters			
Set	2951	2956	3004	3009	A	B	C	D
1	$\surd$	$\surd$	$\surd$	$\surd$	21.91	37.94	7.71	8.37
2	$-$	$-$	$-$	$-$	5.52	88.68	7.72	9.17
3	$-$	$-$	$\surd$	$\surd$	12.02	52.44	7.71	9.23
4	$\surd$	$\surd$	$-$	$-$	21.84	38.07	7.72	8.38
5	$\surd$	$-$	$-$	$\surd$	18.02	43.35	7.73	8.86

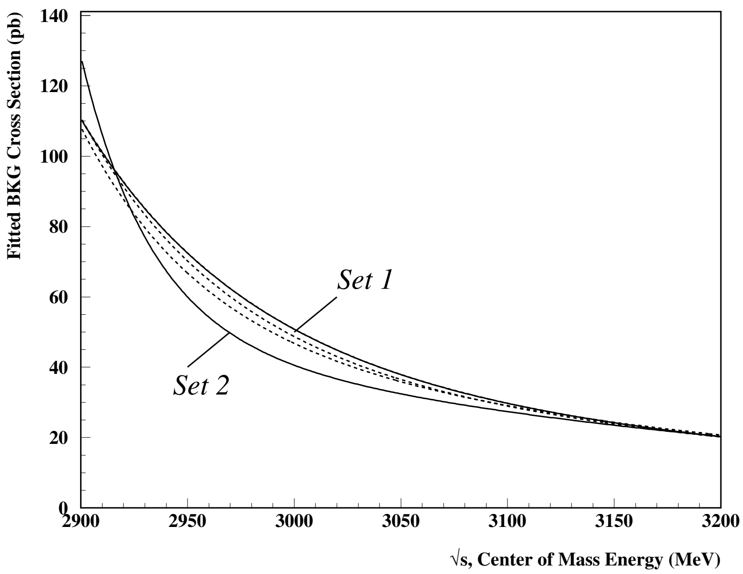

Figure 8.9: Results of fitting the background function (Eq. 8.7) to the data for $|\cos\theta^*| \leq 0.2$. Each fit represents one of the options presented in Table 8.1. Those representing the extreme parameter sets 1 and 2 are indicated explicitly.

and background points, to the sum of the background cross section of the form of (Eq.8.7) and the Breit-Wigner resonance function, to simultaneously determine the best fit background and resonance parameters.

8.2 Determination of Resonance and Background Parameters

The resonance parameters of the charmonium states for which we report measurements have been obtained by use of a Maximum Likelihood fit to the data. The likelihood function,

$$L = \prod_{i=1,N} \frac{\nu_i^{n_i} e^{-\nu_i}}{n_i!}, \tag{8.8}$$

is the product of N Poisson functions (N = the number of data points over which the fit is performed). The term for the ith data point gives the probability that n_i events are observed if ν_i are expected. For a resonance R, the ν_i are given by

$$\nu_i = \left[\int \mathcal{L}\right]_i \times \left(\epsilon_i \alpha \int_0^\infty g_{beam}(E - \sqrt{s}_i)\sigma_{BW}(E)dE + \sigma_{bkg}\right), \tag{8.9}$$

where $\left[\int \mathcal{L}\right]_i$ is the integrated luminosity taken at the ith data point, ϵ_i and α are the overall efficiency and acceptance, respectively. $g_{beam}(E - \sqrt{s}_i)$ is the measured distribution of the CM energy about the mean CM energy $\sqrt{s}_i$, and σ_{BW} is the Breit-Wigner cross section

$$\sigma_{BW}(E) = \frac{4\pi(2J+1)}{E^2 - 4m_p^2} \frac{B(R \to \bar{p}p) \times B(R \to \gamma\gamma)}{1 + 4(E - M_R)^2/\Gamma_R^2}. \tag{8.10}$$

The background cross section, σ_{bkg} is parameterized as in Eq. 8.7. Thus, the parameters of the fit function are the resonance mass M_R, its total width Γ_R and the product of $\bar{p}p$ and $\gamma\gamma$ branching fractions $B(R\rightarrow\bar{p}p) \times B(R\rightarrow\gamma\gamma)$ (or, equivalently, $B(R\rightarrow\bar{p}p) \times \Gamma(R\rightarrow\gamma\gamma)$), and the four background parameters A, B, C and D.

The fit is performed using the CERNLIB routine MINUIT, [57] which finds the point in parameter space which maximizes the natural log of the likelihood function ($ln\ L$). When a maximum is found, the free parameters are each individually varied about the optimum values, while the others are kept constant. The variation in each parameter which results in a change of $ln\ L$ by 1/2 (i.e., $ln\ L$ decreases to $ln\ L_{max} - 1/2$) is reported by MINUIT as the one-σ error on that parameter.

8.3 Resonance Parameters of η_c

The observed $\bar{p}p\rightarrow\gamma\gamma$ cross sections for $|cos(\theta^*)| \leq 0.20$ for the scan across the η_c mass region are shown in Fig. 8.10 as a function of the center of mass energy, $\sqrt{s}$. The data have been fitted, as described above, with all three Breit-Wigner parameters, and all four background parameters allowed to vary in the fit. The solid curve which is superimposed on the data in Fig. 8.10 is the result of this fit.

Our results for the η_c resonance parameters are:

$$\begin{aligned} M(\eta_c) &= 2982.4^{+2.3}_{-2.2} \text{ MeV} \\ \Gamma(\eta_c) &= 26.9^{+10.8}_{-9.5} \text{ MeV} \\ B(\eta_c\rightarrow\bar{p}p) \times B(\eta_c\rightarrow\gamma\gamma) &= 25.3^{+4.6}_{-4.5} \times 10^{-8}. \end{aligned} \tag{8.11}$$

or, equivalently,

$$B(\eta_c\rightarrow\bar{p}p) \times \Gamma(\eta_c\rightarrow\gamma\gamma) = 6.8^{+3.5}_{-2.8} \text{ eV} \tag{8.12}$$

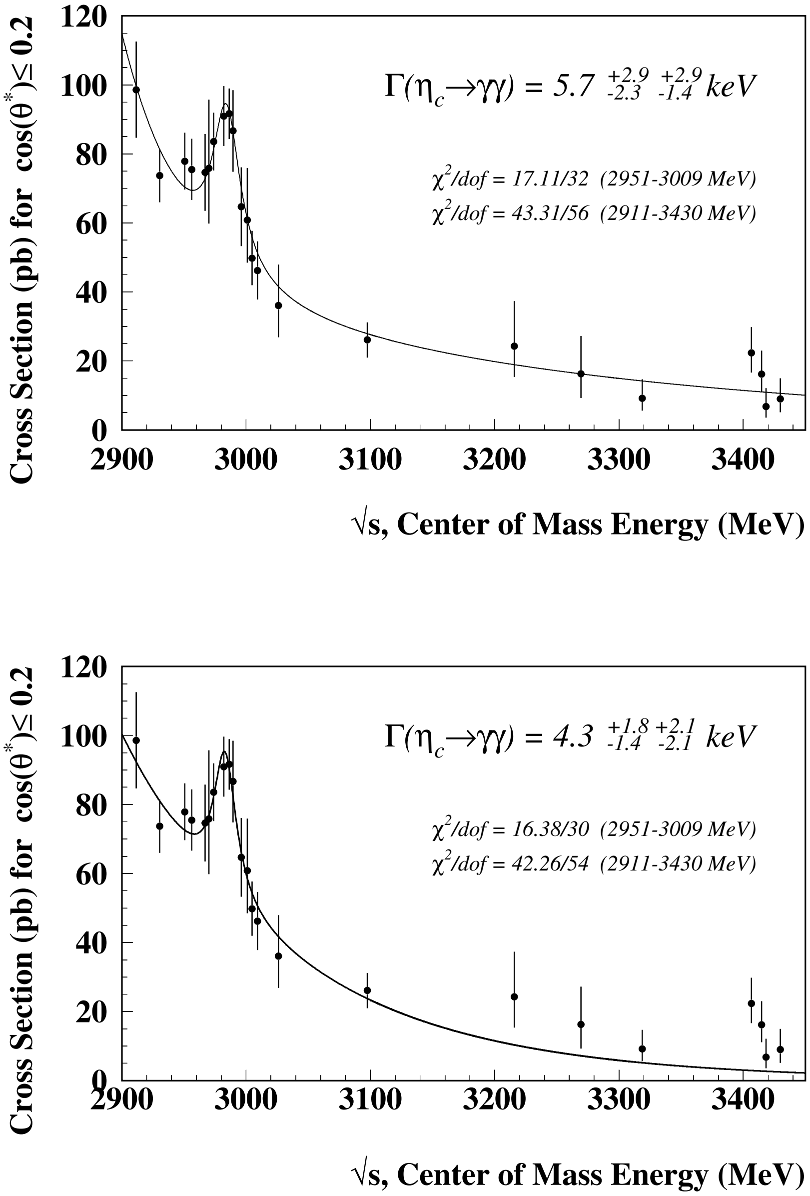

Figure 8.10: Measured cross sections for $\bar{p}p \to \gamma\gamma$ for $|\cos\theta^*| \leq 0.2$ in the η_c region. (top) Our present best fit, to all data points from $\sqrt{s} = 2911$ to 3859 MeV, with all resonance and background parameters free. (bottom) The result of the fit to the data points in the limited region from $\sqrt{s} = 2911$ MeV to 3100 MeV, using the E760 form of the background parameterization. The values of $\chi^2/d.o.f$ for each fit are indicated, calculated for all data points shown, and for the peak (2951-3009 MeV) region.

Table 8.2: Values of η_c resonance parameters from PDG94, [58] E760 [50] and E835. It should be noted that the E760 results are those which were determined by essentially fixing the background to the values determined by the feeddown calculation, a procedure which results in substantially lower errors.

Parameter	**PDG94**	**E760** (≤ 0.25)	**E760** (≤ 0.20)	**E835** (≤ 0.20)
$M(\eta_c)$ (MeV)	2979.8 ± 1.9	$2988.3^{+3.3}_{-3.1}$	$2988.8^{+2.4}_{-2.2}$	$2982.4^{+2.3}_{-2.2}$
$\Gamma(\eta_c)$ (MeV)	$10.3^{+3.8}_{-3.4}$	$23.9^{+12.6}_{-7.1}$	$19.0^{+8.0}_{-5.2}$	$26.9^{+10.8}_{-9.5}$
$B_{\bar{p}p} \times B_{\gamma\gamma} \times 10^8$	68^{+42}_{-31}	$33.6^{+8.0}_{-7.0}$	$44.9^{+10.2}_{-8.8}$	$25.3^{+4.6}_{-4.5}$
$B_{\bar{p}p} \times \Gamma(\eta_c \to \gamma\gamma)$ (eV)		$8.1^{+2.9}_{-2.0}$	$8.6^{+2.5}_{-1.9}$	$6.8^{+3.5}_{-2.8}$
$B_{\bar{p}p} \times 10^4$	12 ± 4			
$B(\eta_c \to \gamma\gamma) \times 10^4$	6^{+6}_{-5}	$2.8^{+0.7+1.4}_{-0.6-0.7}$	$3.0 \pm 0.8^{+1.4}_{-0.8}$	$2.1 \pm 0.4^{+1.1}_{-0.5}$
$\Gamma(\eta_c \to \gamma\gamma)$ (keV)	$7.2^{+2.0}_{-1.7}$	$6.7^{+2.4+3.4}_{-1.7-1.7}$	$7.2^{+2.1+3.6}_{-1.6-1.8}$	$5.7^{+2.9+2.9}_{-2.3-1.4}$
Signal events†		80	77	260

† Events in $2911 \leq \sqrt{s}(\text{MeV}) \leq 3100$ region

We note that the errors on Eq. 8.12 are *not* obtained by dividing Eq. 8.11 by $\Gamma(\eta_c)$. They are obtained by a separate fit.

The best fit values for the background parameters for this fit are:

$$A = 12.5^{+11.41}_{-7.73} \text{ pb} \quad B = 59.0^{+39.2}_{-22.5}$$

$$C = 7.68^{+0.43}_{-0.41} \text{ pb} \quad D = 8.80^{+1.27}_{-1.58}$$

The errors quoted for the resonance parameters of η_c have been obtained by Monte Carlo evaluation, as described in Appendix D. The errors obtained by the Maximum Likelihood fit are only slightly different: $M(\eta_c) = 2982.4^{+2.2}_{-2.4}$ MeV, $\Gamma(\eta_c) = 26.9^{+12.1}_{-8.5}$ MeV, $B(\eta_c \to \bar{p}p) \times B(\eta_c \to \gamma\gamma) = 25.3^{+4.6}_{-4.5} \times 10^{-8}$, $B(\eta_c \to \bar{p}p) \times$

$\Gamma(\eta_c \to \gamma\gamma) = 6.2^{+4.0}_{-2.4}$ eV. For our final results, we use the errors determined by Monte Carlo evaluation.

The resonance parameters are given in Table 8.2, together with the PDG94 averages [58] (which did not include E760 results) and E760 results for both $|cos\theta^*| \leq 0.25$ and $|cos\theta^*| \leq 0.2$. [50]

We recall that the E760 results were obtained by using background parameters which were essentially fixed to the values obtained by using the feed-down calculation. This resulted in errors on $\Gamma(\eta_c)$, $B(\eta_c \to \bar{p}p) \times B(\eta_c \to \gamma\gamma)$, and $B(\eta_c \to \bar{p}p) \times \Gamma(\eta_c \to \gamma\gamma)$ which were $\sim 30\%$ to 50% smaller than those obtained without this 'fixing'. This should be kept in mind when comparing the present results with those of E760.

In order to carry the comparison with E760 one step closer, we have also fitted our data in the limited region near η_c, from 2911 to 3100 MeV, using the functional form for the background used in E760, $\sigma_{bkg} = A \times (\sqrt{s_0}/\sqrt{s})^B$. The results for the η_c resonance and background parameters using this method are:

$$M(\eta_c) = 2982.99^{+2.23}_{-2.14} \text{ MeV}$$
$$\Gamma(\eta_c) = 22.4^{+8.4}_{-6.9} \text{ MeV}$$
$$B(\eta_c \to \bar{p}p) \times B(\eta_c \to \gamma\gamma) = 22.9^{+4.1}_{-3.9} \times 10^{-8}$$
$$B(\eta_c \to \bar{p}p) \times \Gamma(\eta_c \to \gamma\gamma) = 5.1^{+2.2}_{-1.7} \text{ eV}$$
$$B(\eta_c \to \gamma\gamma) = 1.9 \pm 0.3^{+1.0}_{-0.5} \times 10^{-4}$$
$$\Gamma(\eta_c \to \gamma\gamma) = 4.3^{+1.8+2.1}_{-1.4-2.1} \text{ keV}$$

$$A = 53.6^{+4.2}_{-4.5} \text{ pb } B = 22.0^{+3.5}_{-3.3}$$

and the result of the fit is shown in Fig. 8.10. (Note that the background parameters obtained by E760 were very similar: $A_{bkg} = 49.0 \pm 1.3$ pb, $B_{bkg} = 23.1 \pm 1.8$) The poor quality of this fit to the measured background in the region beyond 3200 MeV is quite clear. As stated earlier we consider it more correct to include our knowledge of the background over the entire region $2900 \leq \sqrt{s}(\mathrm{MeV}) \leq 3800$ in the fitting procedure, and we therefore do not include the above results in Table. 8.2.

The stability of the each of the measured quantities with respect to the choice of $\cos(\theta^*)$ cut was checked by varying the value of the cut from 0.12 to 0.40 in eight steps and performing a fit for each $|\cos\theta^*|$ cut value. As is shown in Fig. 8.11, the results for each resonance parameter are quite stable with respect to the choice of cut value.

8.3.1 The η_c Mass

Our result for the η_c mass, $2982.4^{+2.2}_{-2.4}$ MeV, is ~ 3.5 MeV larger than the PDG94 average, and ~ 5.5 MeV smaller than the value reported by E760. Unfortunately, the excellent precision in beam energy determination does not help in this measurement, and the errors on our measurement arise primarily from the fit. The fact that our result for the mass, $M(\eta_c) = 2982.4^{+2.3}_{-2.2}$ MeV differs by two σ from the E760 final result of $M(\eta_c) = 2988.3^{+3.3}_{-3.1}$ is somewhat disturbing, though perhaps not unexpected because of the limited statistical precision of both data sets.

The errors on our mass measurement are comparable to those for the most precise results of other experiments. Our result is shown together with those from other experiments in Fig. 8.12 and Table 8.3.

Our result agrees with that of the Crystal Ball experiment [63] within 1σ.

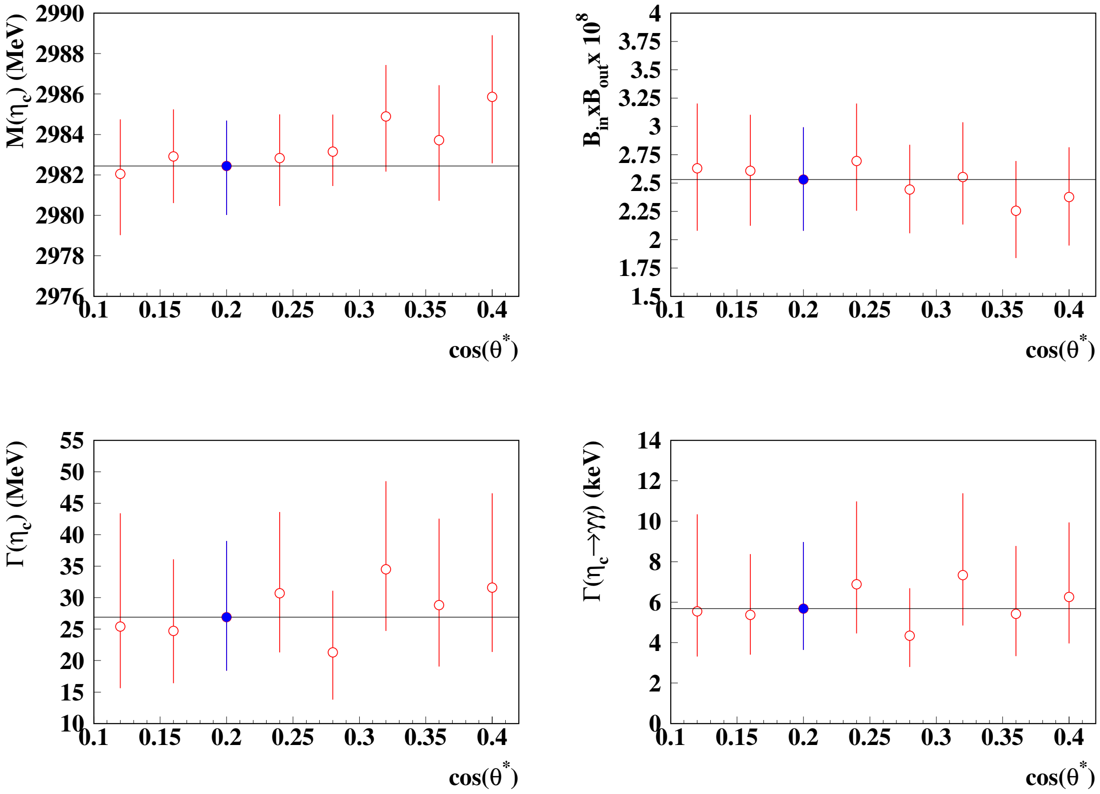

Figure 8.11: Results of a study of the stability of the results for each of the η_c resonance parameters due to the choice of $\cos(\theta^*)$ cut value. The solid circle and the horizontal line in each plot indicate our final results.

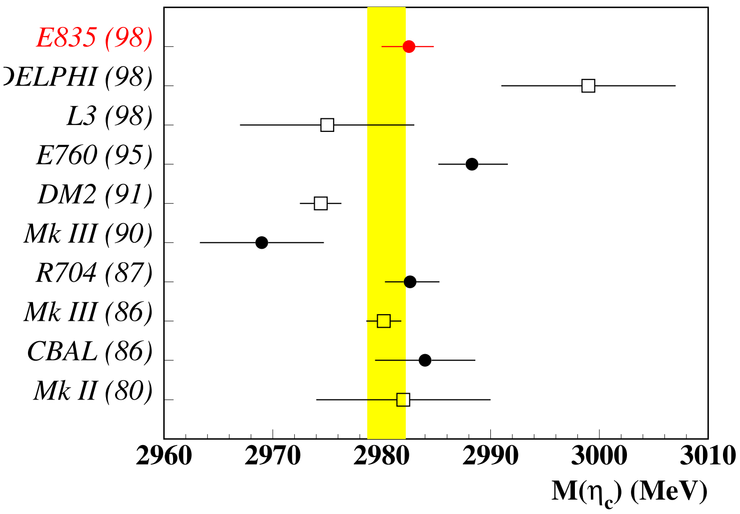

Figure 8.12: Results of measurements of the η_c mass, for comparison to that obtained in E835. The shaded band indicates the weighted average of the displayed results The results indicated by the open squares are from experiments which observed η_c in several hadronic decay channels, and presented the average reconstructed mass as their result. The solid circles indicate results from experiments which measure the η_c mass via a single decay channel.

Table 8.3: Experimental results for the mass of η_c. The weighted averages presented have been calculated according to the method prescribed in PDG98. [2]

Result (MeV)	Experiment (year)	Events	Measurement	Reference
$2982.4^{+2.3}_{-2.2}$	E835 (99)	260	$\bar{p}p \rightarrow \gamma\gamma$	
$2988.3^{+3.3}_{-3.1}$	E760 (95)	76	$\bar{p}p \rightarrow \gamma\gamma$	[50]
2974.4 ± 1.9	DM2 (91)	439	$J/\psi \rightarrow \eta_c \gamma^*$	[59]
$2969 \pm 4 \pm 4$	MkIII (90)	80	$J/\psi \rightarrow \gamma \mathrm{K}^+\mathrm{K}^-\mathrm{K}^+\mathrm{K}^-$	[60]
$2982.6^{+2.7}_{-2.3}$	R704 (87)	12	$\bar{p}p \rightarrow \gamma\gamma$	[61]
2980.2 ± 1.6	MkIII (86)	430	$J/\psi \rightarrow \eta_c \gamma^*$	[62]
$2984 \pm 2.3 \pm 4.0$	CBAL (86)		$J/\psi, \psi' \rightarrow \gamma X$	[63]
2982 ± 8	MkII (80)	18	$\psi' \rightarrow \eta_c \gamma^*$	[64]
2980.2 ± 1.7		Weighted Average		

* Average of several decay modes

The world average is pulled down, however, largely by the DM2 measurement of 2974.4 ± 1.9, and by the Mark III result of 2980.2 ± 1.6. Each of these experiments observed η_c candidates in several hadronic decay modes, and report an average of the reconstructed invariant masses derived from each channel. The statistics in the individual channels range typically from 10 to 50 counts, with a channel or two having over 100 candidates.

Our measurement, and that of E760 and R704, is derived from a scan of the directly-produced resonance, as described in Chapter 4. We observe just one final state, $\gamma\gamma$, and do not reconstruct any invariant mass. Therefore, we do not depend on the knowledge of reconstruction efficiencies and the acceptances for multiple hadronic final states, as do experiments like DM2 and Mark III. Errors in the determination of the momenta and energies of final state particles, and uncertainties in particle identification can affect the results obtained by such a method. This may explain the apparent disagreement between results from this type of experiment and experiments like ours in which η_c is observed in a single decay mode.

One of the important observables of the charmonium system is the hyperfine splitting. The $1S$ hyperfine splitting of charmonium system is the mass difference between $J/\psi(1^3S_1)$ and $\eta_c(1^1S_0)$. We find it to be

$$\Delta M_{1S} = 3096.88 \pm 0.04 \text{ MeV } - 2982.4^{+2.3}_{-2.2} \text{ MeV } = 114.5^{+2.3}_{-2.2} \text{ MeV}. \tag{8.13}$$

Predictions of the mass of η_c' (or rather the 2S splitting $\Delta m = m(\psi') - m(\eta_c'))$ are based upon the $J/\psi - \eta_c$ mass difference. We discuss this later in Sec. 8.6.

8.3.2 The Total Width of η_c

Our result for the η_c total width, $\Gamma(\eta_c) = 26.9^{+10.9}_{-9.5}$ MeV, is significantly larger than that from other experiments, with the exception of the E760 result of $23.9^{+12.6}_{-7.1}$. Though we expended $\sim 20pb^{-1}$ in the η_c region (i.e. from 2900 MeV to 3100 MeV), reflecting a 6-fold increase in luminosity over E760, the errors in our width measurement have not improved significantly from those on the E760 result. This is largely due to the poor statistics for the background points. Our result, together with width results from other experiments, is presented in Table 8.4 and in Fig. 8.13 to allow comparison with other experimental results. It is apparent that none of the reported measurements of the total width are particularly precise. Other than our own E760/E835 measurements, the only measurement which has $\leq \pm 50\%$ error is that from the Crystal Ball experiment. [63]. The difference between the results of η_c width by E760/E835, which range from 20 to 30 MeV, and the Crystal Ball experiment, $\Gamma(\eta_c) = 11.5 \pm 4.5$, is large, and warrants some discussion.

The Crystal Ball result depends not only on the statistics, but on the knowledge of the energy resolution of the photon detector, while ours does not. Therefore any error in the determination of the energy resolution may have a bearing on the Crystal Ball width measurement. The inclusive photon spectrum obtained by Crystal Ball is presented in Fig. 8.14. The three panels of the figure represent three different selections of data.

The Crystal Ball claims an intrinsic photon resolution (FWHM) of $\Gamma = 12 \pm 1$ MeV for the ~ 108 MeV photons from $J/\psi \rightarrow \gamma \eta_c$. Their reported total width of

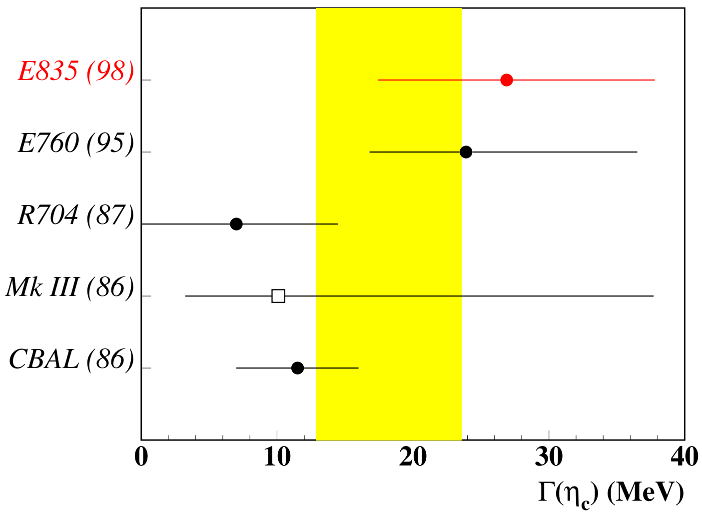

Figure 8.13: Experimental measurements of the η_c total width, for comparison to the E835 result. The shaded band indicates the weighted average of the displayed results. The Mark III result, indicated with the open square, is shown with errors corresponding to a 90% confidence interval.

Table 8.4: Experimental results for $\Gamma(\eta_c)$. The weighted averages presented have been calculated according to the method prescribed in PDG98. [2]

Result (MeV)	Experiment (year)	Events	Measurement	Reference
$26.9^{+10.8}_{-9.5}$	E835 (99)	260	$\bar{p}p\to\gamma\gamma$	
$24.3^{+12.6}_{-7.1}$	E760 (95)	76	$\bar{p}p\to\gamma\gamma$	[50]
$7.0^{+7.5}_{-7.0}$	R704 (87)	12	$\bar{p}p\to\gamma\gamma$	[61]
$10.1^{+33.0}_{-8.2}$	MkIII (86)	23	$J/\psi\to\gamma\bar{p}p^*$	[62]
11.5 ± 4.5	CBAL (86)		$J/\psi, \psi'\to\gamma X$	[63]
18.2 ± 5.3	Weighted Average			

* Errors correspond to 90% confidence interval.

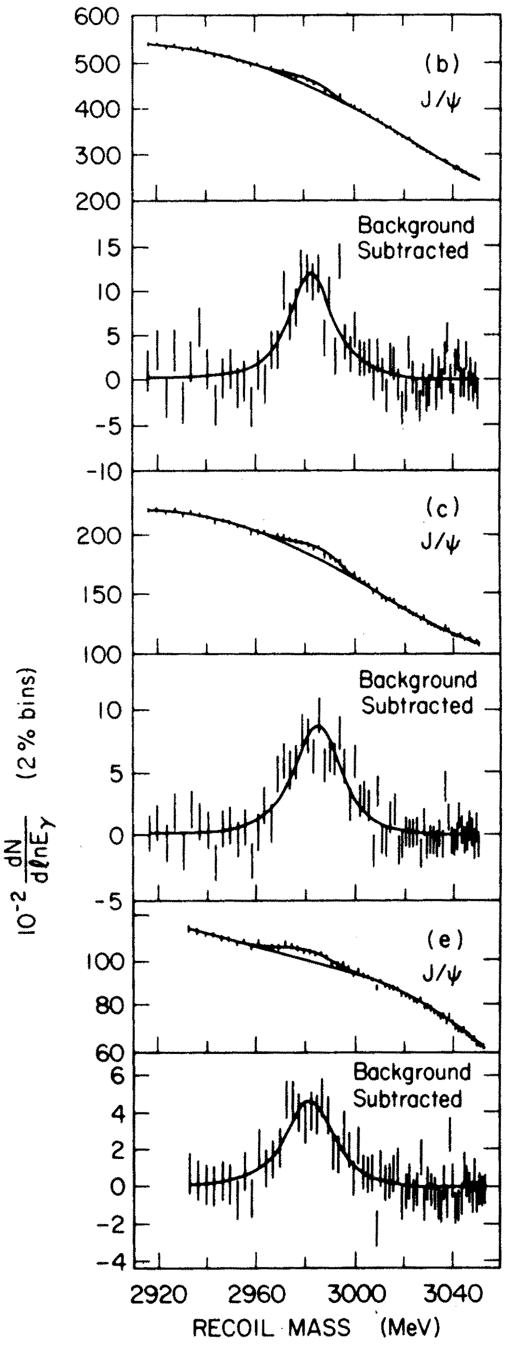

Figure 8.14: Inclusive photon spectra from $J/\psi \to \gamma X$ obtained by the Crystal Ball. The three sets of panels, indicated by (b), (c) and (e), represent three different selections of their data.

η_c, $\Gamma(\eta_c) = 11.5 \pm 4.5$ MeV, added in quadrature would lead to an observed width of ~ 17 MeV. However, the fits presented in Fig. 8.14 appear to have FWHM of $\sim 20 - 22$ MeV, which corresponds to a $\sim 50\%$ larger width than quoted. On the other hand, we cannot rely on the widths estimated from a figure in order to critique the Crystal Ball measurement.

It is apparent from Fig. 8.14 that the Crystal Ball measurements have a signal to background ratio of $\sim 1 : 20$. Despite large statistics, background subtraction in such cases can be problematic and non-unique. This could also contribute to uncertainty in the width measurement by the Crystal Ball.

To be fair, we must point out once again that our own results for $\Gamma(\eta_c)$ depends rather sensitively on how we parameterize and fit the background. The width was found to vary between ~ 20 and ~ 33 MeV depending on which background set of Table 8.1 was used. We conclude that an improved direct measurement of the all-important width of η_c is possible with the $\bar{p}p$ annihilation technique, but only if hardware improvements to substantially reduce the feed-down background are made, and background is measured with high statistical precision over a wide range of energies about η_c.

8.3.3 The Two Photon Partial Width of η_c

We have measured the product $B(\eta_c \to \bar{p}p) \times \Gamma(\eta_c \to \gamma\gamma)$ to be

$$B(\eta_c \to \bar{p}p) \times \Gamma(\eta_c \to \gamma\gamma) = 6.8^{+3.5}_{-2.8} \text{ eV}. \tag{8.14}$$

We obain the two photon partial width of η_c by dividing this by the PDG value for the branching fraction $B(\eta_c \to \bar{p}p) = (1.2 \pm 0.4) \times 10^{-3}$. [2] Thus,

$$\Gamma(\eta_c \to \gamma\gamma) = 5.7^{+2.9+2.9}_{-2.3-1.4} \text{ keV}. \tag{8.15}$$

The first error on $\Gamma(\eta_c \to \gamma\gamma)$ is statistical, while the second is the asymmetric error which arises from the 33% error on the branching fraction $B(\eta_c \to \bar{p}p)$. (See Appendix D) The result of the present measurement is shown for comparison with results from other measurements in Fig. 8.15 and Table 8.5. All measurements of $\Gamma(\eta_c \to \gamma\gamma)$, other than those of E835, E760 and R704, come from photon-photon fusion experiments. A short description of these experiments is therefore in order.

$\gamma\gamma$ Fusion Experiments

Experiments like CLEO and the LEP experiments can produce C-even charmonium states, like $\eta_c(J^{PC} = 0^{-+})$ and $\chi_2(J^{PC} = 2^{++})$, in $\gamma\gamma$ fusion, *i.e.*, in the reaction

$$e^+e^- \to e^+e^-\gamma\gamma,\ \gamma\gamma \to (c\bar{c}) \to hadrons. \tag{8.16}$$

Such experiments must contend with low effective luminosity for the $\gamma\gamma$ interaction. Two examples of results on charmonium states from $\gamma\gamma$ fusion at CLEO are shown in Fig. 8.16.

$\gamma\gamma$ fusion experiments offer a logical choice for the measurement of $\gamma\gamma$ partial widths, for they measure $\Gamma(R \to \gamma\gamma)$, rather than $B(R \to \gamma\gamma)$. However, the event statistics in these experiments are usually poor and spread over several decay channels whose branching ratios are also poorly known. For example, for η_c, no branching

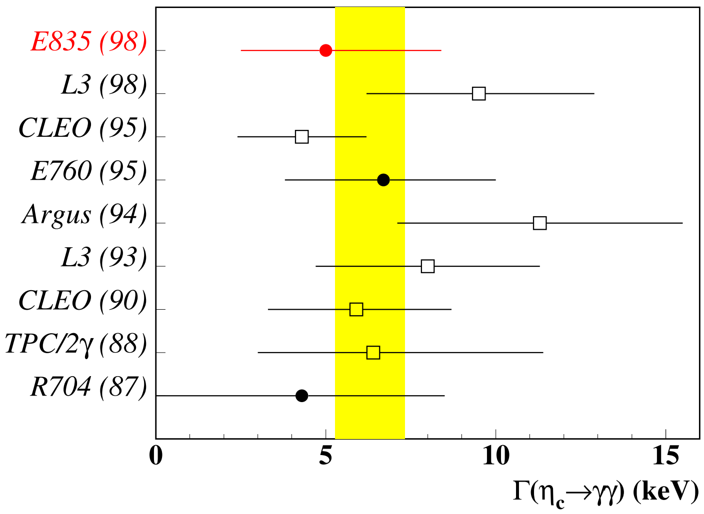

Figure 8.15: Experimental measurements of $\Gamma(\eta_c \to \gamma\gamma)$, for comparison to the E835 result. The shaded band indicates the weighted average of the displayed results. The open squares indicate results from $\gamma\gamma$ fusion experiments. The solid circles indicate results from $\bar{p}p$ annihilation experiments.

Table 8.5: Experimental results for $\Gamma(\eta_c \to \gamma\gamma)$. The weighted average presented has been calculated according to the method prescribed in PDG98. [2]

Result (keV)	Experiment (year)	Events	Measurement	Reference
$5.7^{+2.9+2.9}_{-2.3-1.4}$	E835(99)	260	$\bar{p}p \to \gamma\gamma$	
$9.5^{+2.1}_{-1.9} \pm 2.7$	L3(98)	108	$\gamma\gamma \to$ *hadrons**	[65]
$4.3 \pm 1.0 \pm 1.6$	CLEO(95)	54	$\gamma\gamma \to \pi^+\pi^- K^\pm \pi^\mp$	[66]
$6.7^{+2.4+3.4}_{-1.7-1.7}$	E760(95)	76	$\bar{p}p \to \gamma\gamma$	[50]
11.3 ± 4.2	Argus(94)	57	$\gamma\gamma \to$ *hadrons**	[67]
$8.0 \pm 2.3 \pm 2.4$	L3(93)	17	$\gamma\gamma \to$ *hadrons**	[68]
$5.9^{+2.1}_{-1.8} \pm 1.9$	CLEO(90)	15	$\gamma\gamma \to$ *hadrons**	[69]
$6.4^{+5.0}_{-3.4}$	TPC/2γ(88)	4	$\gamma\gamma \to$ *hadrons**	[70]
$4.3^{+3.4+2.2}_{-3.7-1.1}$	R704(86)	12	$\bar{p}p \to \gamma\gamma$	[61]
6.3 ± 1.0	Weighted Average			

* Average of several decay modes

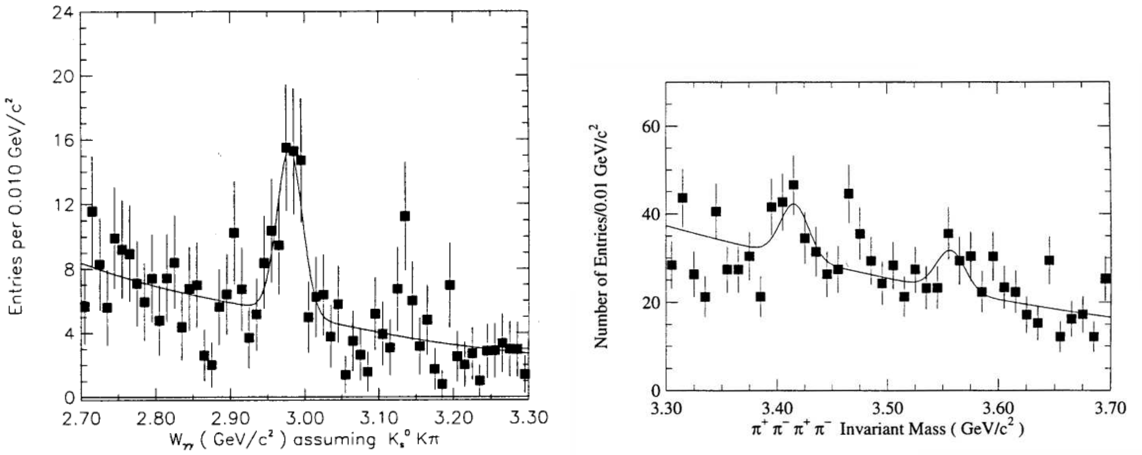

Figure 8.16: Invariant mass spectra from CLEO [66], showing their evidence for (left)η_c and (right) χ_0 and χ_2 produced in $\gamma\gamma$ fusion.

fraction has been measured to better than $\sim \pm 30\%$. Nevertheless, we wish to review the results from these experiments.

Because η_c is the ground state of charmonium, all hadronic decays are forbidden by the Zweig rule, and they have small branching ratios. Photon-photon fusion experiments must detect η_c in these weak and poorly-measured hadronic decay channels. Before E760, there were no reported measurements of $\Gamma(\gamma\gamma \to \eta_c)$ which had more than ~ 20 events in a single hadronic decay mode. Since then, single-channel statistics have improved. We consider the most recent $\gamma\gamma$ measurement, reported by the L3 experiment at CERN at ICHEP '98 [74] in some detail here.

The L3 collaboration reported a measurement of $\Gamma(\eta_c \to \gamma\gamma) = 9.5^{+2.1}_{-1.9} \pm 2.7$ keV based on the observation of 108 ± 21 events spread over ten hadronic decay channels. Of these ten channels, five did not show any excess above the expected background in the η_c mass region. We reproduce the L3 results in Table 8.6

Table 8.6: Summary of experimental results for η_c produced in $\gamma\gamma$ fusion at the L3 experiment.

Channel	N_{evt}	$\Gamma(\eta_c \to \gamma\gamma)$
$\eta_c \to \pi^+\pi^-\pi^+\pi^-$	$47.5^{+16.1}_{-14.5} \pm 4.9$	$8.6^{+2.9}_{-2.6}$ keV
$\eta_c \to K^0 K^\pm \pi^\mp$	$15.8^{+6.6}_{-6.2} \pm 1.1$	$7.5^{+3.2}_{-2.9}$ keV
$\eta_c \to \eta(\to\gamma\gamma)\pi^+\pi^-$	$5.4^{+2.6}_{-2.1} \pm 0.08$	$9.4^{+4.5}_{-3.6}$ keV
$\eta_c \to \pi^0 \mathrm{K}^+\mathrm{K}^-$	$13.8^{+6.5}_{-5.4} \pm 0.9$	31^{+16}_{-15} keV
$\eta_c \to \eta'(\to\rho\gamma)\pi^+\pi^-$	$25.1^{+9.1}_{-8.2} \pm 2.8$	$48.8^{+17.8}_{-16.0}$ keV
$\eta_c \to \mathrm{K}^+\mathrm{K}^-\pi^+\pi^-$	< 34.5	-
$\eta_c \to \rho^+\rho^-$	< 12.5	-
$\eta_c \to \phi\phi$	< 7.8	-
$\eta_c \to \eta'(\to\eta\pi\pi)$	< 4.7	-
$\eta_c \to \eta(\to 3\pi)$	< 4.2	-
overall	$\sim 108 \pm 21$	$9.5^{+2.1}_{-1.9} \pm 1.7$

There are several difficulties which all $\gamma\gamma$ fusion experiments face. First, the reconstruction of η_c in hadronic decay channels requires the detection of several low-mass and low p_T hadrons, and/or photons, while the detectors (like L3) are optimized for looking at high p_T particles. Related to this is the problem of determining trigger efficiencies for these low-p_T events. Finally, because η_c is observed in several decay channels, the efficiencies and acceptances for event selection and reconstruction for all the channels need to be determined accurately. This is a daunting task.

To summarize, we note that, despite their relatively large errors, the results from the three $\bar{p}p$ annhilation experiments, E835, E760 and R704, are consistent - their average is 5.6 ± 1.8 keV. Other experimental results have errors of $\sim 40\%$ each, but are also consistent, with the present world average being $\Gamma(\eta_c \to \gamma\gamma) = 6.3 \pm 1.0$ keV.

8.4 The Two Photon Partial Width of χ_2

E760 reported a measurement of $\Gamma(\chi_2 \to \gamma\gamma) = 0.321 \pm 0.078 \pm 0.054$ [71] which differed significantly from the previous world average. [72] Most of the previous determinations of the $\gamma\gamma$ partial width of χ_2 came from $\gamma\gamma$-fusion experiments, such as CLEO, [73][66] and all these measurements appeared to be consistent with each other, and much larger (albeit with large statistical errors) than the E760 result. It was therefore considered important to measure $\Gamma(\chi_2 \to \gamma\gamma)$ again.

We have made a measurement of $\Gamma(\chi_2 \to \gamma\gamma)$ in E835 with approximately $8.4pb^{-1}$ of integrated luminosity near the χ_2 peak, compared to $\sim 2.6pb^{-1}$ in E760. The cross sections for $\bar{p}p \to \gamma\gamma$ in this region are shown in Fig. 8.17. The total width $\Gamma(\chi_2) = 1.98 \pm 0.18$ MeV, the $\bar{p}p$ branching fraction $B(\chi_2 \to \bar{p}p) = 1.0 \pm 0.1 \times 10^{-4}$ and the mass $M(\chi_2) = 3556.16 \pm 0.14$ MeV were each well measured in E760 in the reaction $\bar{p}p \to \chi_2 \to \gamma J/\psi$. In the present analysis we have fixed $\Gamma(\chi_2)$ and $B(\chi_2 \to \bar{p}p)$ to the above values. To allow for errors in the overall energy scale determined by our beam momentum measurements, we have allowed the mass $\mathrm{M}(\chi_2)$ to vary in the fit.

From the fit to our data, we obtain

$$B(\chi_2 \to \bar{p}p) \times B(\chi_2 \to \gamma\gamma) = 1.72 \pm 0.26 \pm 0.04 \times 10^{-8}, \tag{8.17}$$

or, equivalently,

$$B(\chi_2 \to \bar{p}p) \times \Gamma(\chi_2 \to \gamma\gamma) = 0.0343^{+0.0053}_{-0.0051} \pm 0.021 \text{ eV}. \tag{8.18}$$

The first errors are statistical,† and the second are systematic errors obtained by

†The errors determined by the fit, and by Monte Carlo evaluation (see Appendix D) are iden-

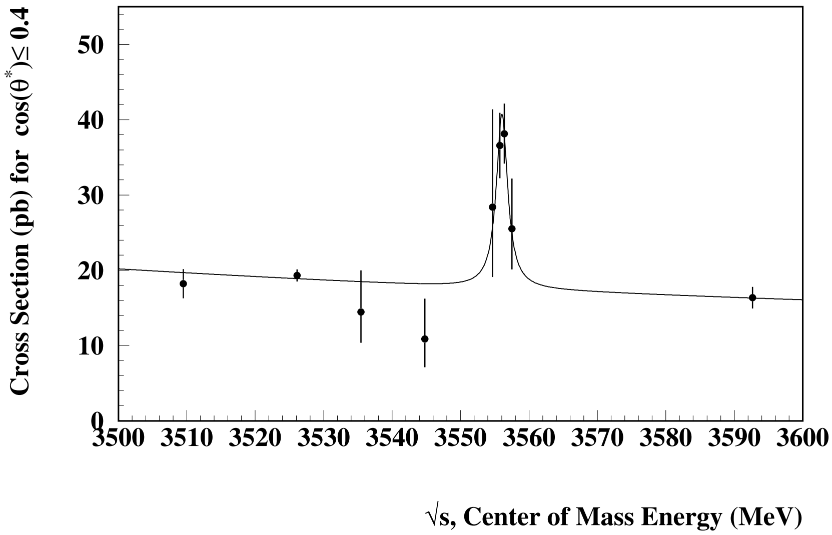

Figure 8.17: Measured cross sections for $\bar{p}p \to \gamma\gamma$ for $|\cos\theta^*| \leq 0.4$ in the χ_2 region.

Table 8.7: Experimental results from E760 and E835 for χ_2. In both E760 and E835 analyses, the total width $\Gamma(\chi_2)$ and the branching fraction $B(\chi_2 \to \bar{p}p)$ were fixed to the values determined by E760 from analysis of the reaction $\bar{p}p \to \chi_2 \to \gamma J/\psi$.

	E760	**E835**
Mass (MeV)	3556.16 ± 0.14	3556.10 ± 0.35
$B(\chi_2 \to \bar{p}p) \times B(\chi_2 \to \gamma\gamma) \times 10^8$	$1.60 \pm 0.39 \pm 0.16^*$	$1.72 \pm 0.26 \pm 0.04$
$B(\chi_2 \to \bar{p}p) \times \Gamma(\chi_2 \to \gamma\gamma)$ (eV)	$0.032 \pm 0.008 \pm 0.004$	$0.0343^{+0.0053}_{-0.0051} \pm 0.021$
$B(\chi_2 \to \bar{p}p) \times 10^4$	$1.0 \pm 0.1^\dagger$	$1.0 \pm 0.1^\dagger$
$B(\chi_2 \to \gamma\gamma) \times 10^4$	$1.6 \pm 0.4 \pm 0.2$	$1.72 \pm 0.26^{+0.19}_{-0.16}$
$\Gamma(\chi_2 \to \gamma\gamma)$ (keV)	$0.321 \pm 0.078 \pm 0.054$	$0.343^{+0.053+0.043}_{-0.051-0.038}$
Signal Events‡	30	87

*The second error given is an estimate of the contribution due to background subtraction.
†Assumed
‡ Events in $3554 \leq \sqrt{s}(MeV) \leq 3558$ region.

varying the 'fixed' $\Gamma(\chi_2)$ between the experimental errors in the fit. Dividing these by the PDG value for the branching fraction $B(\chi_2 \to \bar{p}p) = 1.0 \pm 0.1 \times 10^{-4}$, we find

$$B(\chi_2 \to \gamma\gamma) = 1.72 \pm 0.26^{+0.19}_{-0.16} \times 10^{-4} \tag{8.19}$$

and

$$\Gamma(\chi_2 \to \gamma\gamma) = 0.343^{+0.053+0.043}_{-0.051-0.038} \text{ keV}. \tag{8.20}$$

Here, the systematic error quoted is the combination of the 10% uncertainty on $B(\chi_2 \to \bar{p}p)$ with the systematic errors in Eq. 8.18 and 8.19. Thus the present measurement confirms the E760 results, and have $\gtrsim$ 30% smaller errors. (see Table 8.7)

If we fit the data allowing the total width $\Gamma(\chi_2)$ to vary as well, we obtain $M(\chi_2) = 3556.07^{+0.45}_{-0.43}$ MeV, $\Gamma(\chi_2) = 2.81^{+2.65}_{-1.10}$, and $B(\chi_2 \to \bar{p}p) \times B(\chi_2 \to \gamma\gamma) = 1.57^{+0.36}_{-0.29} \times 10^{-8}$. We note that despite the poor determination of width because of the lack of data in the wings of the resonance, the branching fraction is very well determined, and agrees with our final results, which were obtained by fixing the width.

From the χ_2 best fit, for $|cos\theta^*| \leq 0.4$, the background parameters are found to be

$$\begin{aligned} A = 311.5^{+16.4}_{-25.0} \text{ pb} \quad B = 24.0^{+2.2}_{-1.8} \\ C = 13.0^{+1.9}_{-2.2} \text{ pb} \quad D = 2.2^{+3.6}_{-3.7}. \end{aligned} \tag{8.21}$$

These background parameters were obtained by fitting all the data from $\sqrt{s} = 2911$ to 3829 MeV. They will be used again to define the background for our analysis of the data in the χ_0 and η_c' regions.

---

tical.

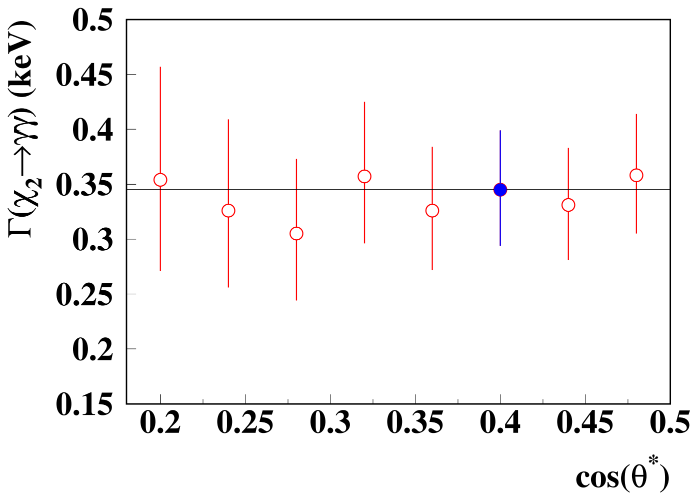

Figure 8.18: Results of a study of the stability of the result for $\Gamma(\chi_2 \to \gamma\gamma)$ relative to the choice of $|\cos\theta^*|$ cut value.

The stability of our present result was checked with respect to the choice of $\cos(\theta^*)$ cut by varying the value of the cut in 8 points from 0.2 to 0.48 and evaluating the partial width. As shown in Fig. 8.18, the result is quite stable.

Our measurement of $\Gamma(\chi_2 \to \gamma\gamma)$ is also shown for comparison with other experimental results in Fig. 8.19 and Table 8.8. Our result is, like that obtained by E760, significantly lower and much more precise than the results from $\gamma\gamma$ fusion measurements.

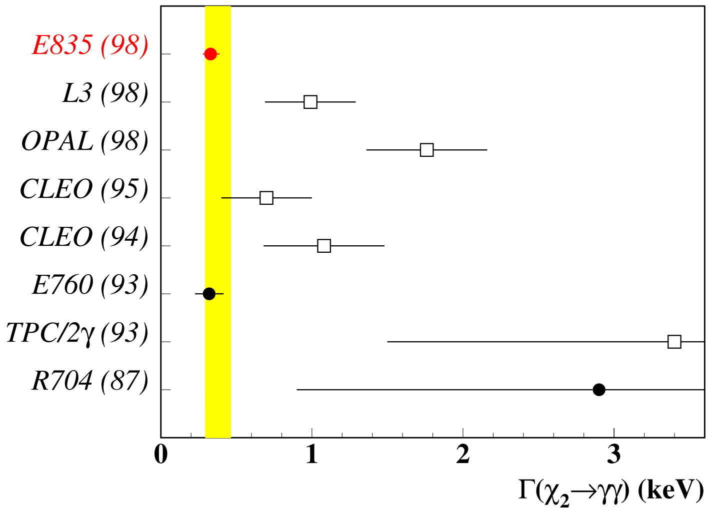

Figure 8.19: Experimental measurements of $\Gamma(\chi_2 \to \gamma\gamma)$, for comparison to the E835 result. The shaded band indicates the weighted average of the displayed results. The open squares indicate results from $\gamma\gamma$ fusion experiments. The solid circles indicate results from $\bar{p}p$ annihilation experiments.

Table 8.8: Experimental results for $\Gamma(\chi_2 \to \gamma\gamma)$. The weighted averages presented have been calculated according to the method prescribed in PDG98. [2]

Result (keV)	Experiment (year)	Events	Measurement	Reference
$0.343^{+0.053+0.043}_{-0.051-0.038}$	E835(99)	87	$\bar{p}p \to \gamma\gamma$	
$1.02 \pm 0.4 \pm 0.17$	L3(98)	12	$\gamma\gamma \to \gamma J/\psi$	[74]
$1.76 \pm 0.47 \pm 0.40$	OPAL(98)	22	$\gamma\gamma \to \gamma J/\psi$	[75]
$0.7 \pm 0.2 \pm 0.2$	CLEO(95)	42	$\gamma\gamma \to 2(\pi^+\pi^-)$	[66]
$1.08 \pm 0.30 \pm 0.26$	CLEO(94)	25	$\gamma\gamma \to \gamma J/\psi$	[73]
$0.321 \pm 0.078 \pm 0.054$	E760(93) [50]	30	$\bar{p}p \to \gamma\gamma$	
$3.4 \pm 1.7 \pm 0.9$	TPC/2γ(93)	6	$\gamma\gamma \to \gamma J/\psi$	[76]
$2.9^{+1.3}_{-1.0} \pm 1.7$	R704(87)	6	$\bar{p}p \to \gamma\gamma$	[61]
0.38 ± 0.08	Weighted Average			

8.5 Measurement of $\bar{p}p \rightarrow \chi_0 \rightarrow \gamma\gamma$

The χ_0 resonance has been observed by us in the reaction $\bar{p}p \rightarrow \gamma J/\psi$, and the results for the χ_0 resonance parameters from that measurement are: [77, 78]

$$M(\chi_0) = 3417.4^{+1.8}_{-1.9} \pm 0.3 \text{ MeV}$$

$$\Gamma(\chi_0) = 16.6^{+5.2}_{-3.7} \pm 0.1 \text{ MeV}$$

$$B(\chi_0 \rightarrow \bar{p}p) = 4.82^{+0.94}_{-0.78} \pm 0.23(^{+2.08}_{-1.12}) \times 10^{-4} \tag{8.22}$$

Since $\Gamma(\chi_0 \rightarrow \gamma\gamma)$ is expected to be larger than $\Gamma(\chi_2 \rightarrow \gamma\gamma)$, we ought to be able to observe χ_0 in the reaction $\bar{p}p \rightarrow \chi_0 \rightarrow \gamma\gamma$. However, we have failed to find evidence for χ_0 in this reaction, largely because of the small value of the luminosity invested in the χ_0 measurements. The measured $\gamma\gamma$ cross sections for $|\cos\theta^*| \leq 0.4$ are plotted for energies between 3200 and 3800 MeV in Fig. 8.20. The curve shows the background fit for $|\cos\theta^*| \leq 0.4$, obtained in Eq. 8.22. It is clear that we do not have sufficient statistics, to claim evidence for χ_0 in these data, but we can set an upper limit on the product $B(\chi_0 \rightarrow \bar{p}p) \times \Gamma(\chi_0 \rightarrow \gamma\gamma)$.

The $\gamma\gamma$ data shown in Fig. 8.20 have been fitted for the product $B(\chi_0 \rightarrow \bar{p}p) \times \Gamma(\chi_0 \rightarrow \gamma\gamma)$, with the mass and total width fixed to the measured values in Eq. 8.23. The background is also fixed to the values presented in Sec. 8.4. Using the method outlined in Appendix D, we have determined a 90% confidence upper limit for $B(\chi_0 \rightarrow \bar{p}p) \times \Gamma(\chi_0 \rightarrow \gamma\gamma)$:

$$B(\chi_0 \rightarrow \bar{p}p) \times \Gamma(\chi_0 \rightarrow \gamma\gamma) \leq 0.63 \text{ eV}, \quad 90\% CL. \tag{8.23}$$

Dividing this by $B(\chi_0 \rightarrow \bar{p}p)$ from Eq. 8.23, we find that

$$\Gamma(\chi_0 \rightarrow \gamma\gamma) \leq 1.3 \text{ keV} \ , \quad 90\% CL. \tag{8.24}$$

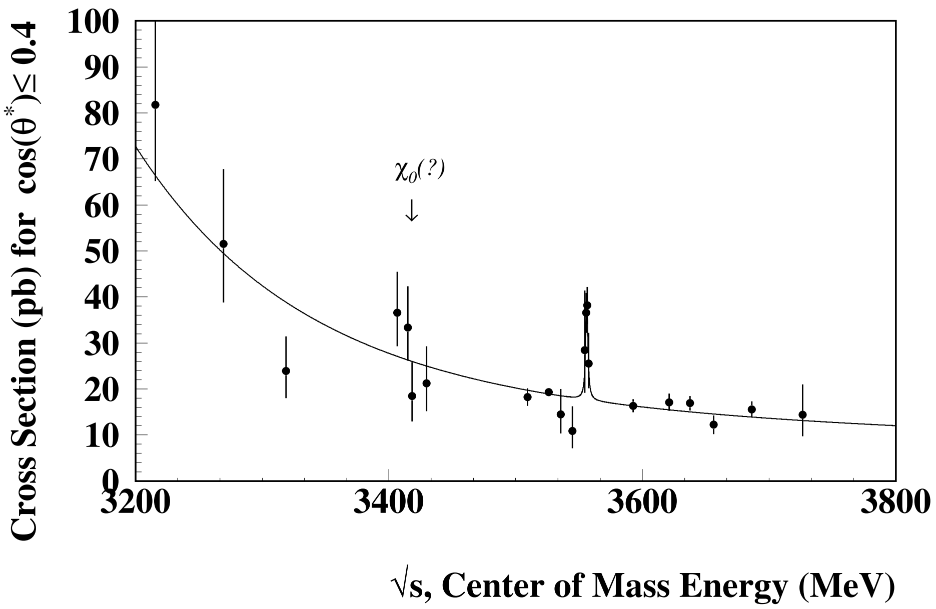

Figure 8.20: Measured cross sections for $\bar{p}p \to \gamma\gamma$ for $|\cos\theta^*| \leq 0.4$ in the χ_0 search region. The solid line is the result of the fit to the background, with the parameters presented in Sec. 8.4. The χ_2 peak at $\sqrt{s} = 3556.18$ MeV is clearly visible. The E835 result for the χ_0 mass, $M(\chi_0) = 3417.4^{+1.8}_{-1.9} \pm 0.3$ MeV, measured in the reaction $\bar{p}p \to \chi_0 \to \gamma J/\psi$, is indicated by the arrow.

This upper limit may be compared with the two measurements of the partial width in the literature, $\Gamma(\chi_0 \to \gamma\gamma) = 4.2 \pm 2.8$ keV) from the Crystal Ball [79] and $\Gamma(\chi_0 \to \gamma\gamma) = 1.7 \pm 0.8$ keV, from CLEO. [80]. The CLEO spectrum is displayed in Fig. 8.16.

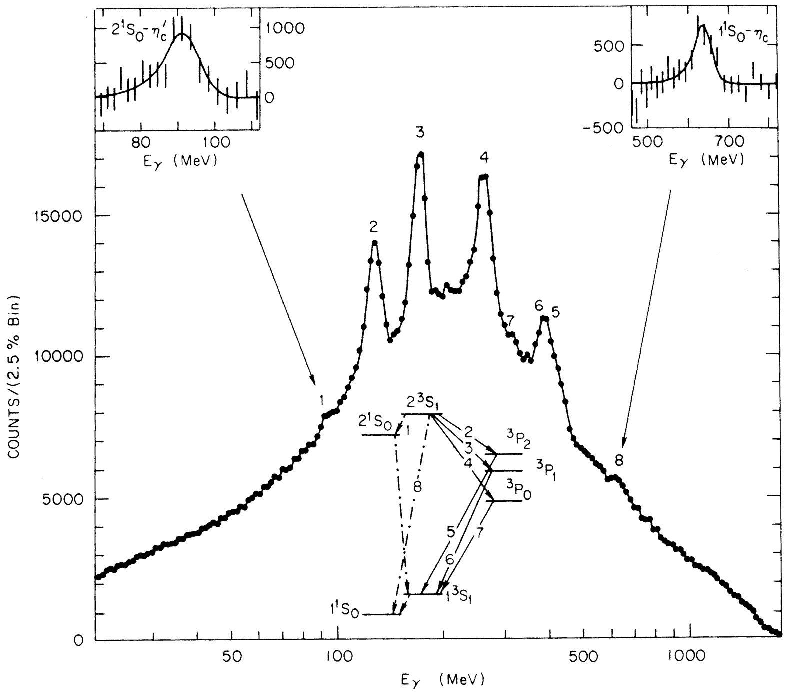

Figure 8.21: Evidence for η_c' in the inclusive photon spectrum from the Crystal Ball. [81] The insets in the upper left and upper right hand parts of the figure are expanded views of the background-subtracted spectrum in the regions corresponding to transitions to η_c' and η_c.

8.6 The Search for η_c'

The radial excitation of $\eta_c(1^1S_0)$, the ground state of charmonium, is $\eta_c'(2^1S_0)$. Its identification has been reported by only one experiment, the Crystal Ball experiment at SLAC. The Crystal Ball observed an excess of events in the inclusive photon spectrum from ψ' [81] at a mean photon energy of 91 ± 5 MeV, which corresponds to a mass of $M(\eta_c') = 3594 \pm 5$ MeV. (see Fig. 8.21.) The Crystal Ball also reported a 95% confidence level upper limit for the total width $\Gamma(\eta_c')$ of 8 MeV. These results for η_c' are not included in the PDG summary tables for lack of any confirming measurements. E760 attempted to identify η_c', but failed. [50] We describe here the results of our search.

Predictions for η_c' mass and width

The choice of the E760/E835 search region for η_c', and the spacing between data points in $\sqrt{s}$ depended not only on the mass and width of the Crystal Ball candidate, but on theoretical estimates of the same. We discuss here theoretical predictions for the η_c' mass and width which motivated the search in E760 and E835.

Predictions for $M(\eta_c')$

Buchmüller and Tye [83] have shown that for $l = 0$, one obtains the familiar form of the hyperfine splitting in a Coulomb potential [1] with only an additional factor for the QCD radiative correction:

$$\Delta M(^3S_1 - {}^1S_0) = \frac{32\pi}{9}\frac{\alpha_{\rm S}}{m_c^2}|\psi(0)|^2\left[1 + 0.77\frac{\alpha_{\rm S}}{\pi}\right]. \tag{8.25}$$

To the same order,

$$\Gamma(V\to e^+e^-) = \frac{16\pi}{9}\frac{{\alpha_{\rm EM}}^2}{m_c^2}|\psi(0)|^2\left[1 - 5.33\alpha_{\rm S}/\pi\right]. \tag{8.26}$$

Thus,

$$\Delta M(^3S_1 - {}^1S_0) = 2\Gamma(V\to e^+e^-) \times \frac{\alpha_{\rm S}}{{\alpha_{\rm EM}}^2}\left[\frac{1 + 0.77\alpha_{\rm S}/\pi}{1 - 5.33\alpha_{\rm S}/\pi}\right]. \tag{8.27}$$

It follows, therefore, that

$$\frac{\Delta M(\psi' - \eta_c')}{\Delta M(J/\psi - \eta_c)} = \frac{\Gamma(\psi'\to e^+e^-)}{\Gamma(J/\psi\to e^+e^-)} = \frac{2.14 \pm 0.21\ \text{keV}}{5.26 \pm 0.38\ \text{keV}} = 0.407 \pm 0.049. \tag{8.28}$$

We note that sometimes m_c in Eq.8.27 is replaced by $(M_V/2)$, while retaining m_c in Eq. 8.26. This has an historical origin (the original formulation by Van Royen and Weisskopf [22]) and is obviously inconsistent. It gives rise to an additional multiplicative factor of 1.416 in Eq. 8.28, so that

$$\frac{\Delta M(\psi' - \eta_c')}{\Delta M(J/\psi - \eta_c)} = 0.576 \pm 0.070. \tag{8.29}$$

With our result of $\Delta M(J/\psi - \eta_c) = 114.5$ MeV, Eq. 8.29 leads to $\Delta M(\psi' - \eta_c') = 46.6 \pm 5.7$ MeV, $M(\eta_c') = 3639 \pm 6$ MeV, and Eq. 8.30 leads to $\Delta M(\psi' - \eta_c') = 66.0 \pm 8.0$ MeV, $M(\eta_c') = 3620 \pm 8$ MeV.

Potential model calculations do not rely on relations such as Eqs. 8.26 and 8.27. They assume potential forms, m_c and α_{S} to fit the masses of one or more charmonium levels, and predict masses and wave functions for various charmonium states. Several such calculations exist in the literature.

Gupta *et al.* [84] use a non-singular $q\bar{q}$ potential with a scalar-vector form of the confining potential, and obtain excellent agreement with the masses of all well-established charmonium states (J/ψ, η_c, ψ', χ_J, h_c, all within ± 5 MeV). They predict $M(\eta_c) = 3622.3$ MeV.

Zhu *et al.* [85] report a relativistic calculation in the Bethe-Salpeter formalism. They fit J/ψ, ψ', $\psi^{(2)}$ and η_c masses within ± 3 MeV, and predict $M(\eta_c') = 3634$ MeV.

Eichten and Quigg [86] have made numerical calculations using several different types of potentials (Buchmüller-Tye, Martin, logarithmic, Cornell) with parameters chosen to reproduce the $M(J/\psi) - M(\eta_c)$ splitting. Their results (renormalized by 2% to account for our determination of $M(\eta_c)$) average to give $M(\eta_c') = 3618 \pm 8$

MeV. Chen and Oakes [87] make an investigation similar to that of Eichten and Quigg with Cornell, logarithmic, and their own 'renormalization-group-improved' potential, and obtain a very similar prediction, $M(\eta_c') = 3620^{+9}_{-12}$ MeV.

A fair summary of the above is that all recent calculations indicate that $M(\eta_c') \approx 3630 \pm 10$ MeV. This is ~ 35 MeV larger than the mass of 3594 ± 5 MeV reported by the Crystal Ball experiment. [81] This sets the stage for our search for η_c'. In the present investigation we scanned the mass region from 3576 to 3660 MeV in order to identify η_c'.

Estimates for $\Gamma(\eta_c')$

A close correspondence between ψ' and η_c' can be drawn as far as the non-annihilation decay channels are concerned. Thus,

$$\begin{aligned} a)\Gamma(\eta_c' \to \gamma(E1) + {}^1P_1) &\;\to\; \Sigma_J \Gamma(\psi' \to \gamma(E1) + {}^3P_J) \approx 80 \text{ keV} \\ b)\Gamma(\eta_c' \to \eta_c + X) &\;\to\; \Gamma(\psi' \to J/\psi + X) \approx 170 \text{ keV} \\ c)\Gamma(\eta_c' \to {}^3P_0 + \pi^0) &\;\to\; \Gamma(\psi' \to {}^1P_1 + \pi^0) \leq 1.3 \text{ keV} \end{aligned} \tag{8.30}$$

Thus the non-annihilation channels of η_c' are not expected to contribute more than 0.3 MeV to its width.

As far as $c\bar{c}$ annihilation channels are concerned, the ${}^1S_0$ states are indeed different from the ${}^3S_1$ states in that the ${}^1S_0$'s must annihilate via two gluons, and the ${}^3S_1$'s via three gluons, leading to the fact that the hadronic decay widths of the ${}^1S_0$'s are larger than those of the ${}^3S_1$'s by big factors of the order of 100. It is therefore not advisable to relate the η_c' hadronic decays directly to those of ψ'. It appears to be more prudent to make the analogy

$$\frac{\Gamma(\eta_c'\to gg)}{\Gamma(\eta_c\to gg)} = \frac{\Gamma(\psi'\to ggg)}{\Gamma(J/\psi\to ggg)} = \frac{46\pm 10 \text{ keV}}{71\pm 6 \text{ keV}} = 0.66\pm 0.15. \tag{8.31}$$

This ratio is in accord with the ratio of the squares of the wave functions of η_c' and η_c (as well as ψ' and J/ψ) calculated in the potential models. Eichten and Quigg [86] have calculated the ratio for several potentials, and their average result is

$$\frac{|\psi(0)|^2(\eta_c')}{|\psi(0)|^2(\eta_c)} = 0.60\pm 0.05. \tag{8.32}$$

Using the experimental ratio in Eq. 8.32, and our determination of $\Gamma(\eta_c\to gg)\approx \Gamma(\eta_c) = 26.9^{+10.8}_{-9.5}$ MeV, we obtain the *estimate* for the η_c' width,

$$\Gamma(\eta_c') \approx \Gamma(\eta_c'\to gg) = 17.8^{+7.1}_{-6.3}\pm 6.1 \text{ MeV}. \tag{8.33}$$

The search for η_c' by E760

E760 searched for η_c' at 6 data points from 3591 to 3621 MeV, They invested a total of $\sim 6pb^{-1}$ of luminosity in the search, and obtained 90% confidence level upper limits on the product of branching ratios of [50]

$$\begin{aligned} B(\eta_c'\to\bar{p}p)\times B(\eta_c'\to\gamma\gamma) &\leq 14.9\times 10^{-8}, \text{ for assumed } \Gamma(\eta_c') = 5 \text{ MeV, and} \\ B(\eta_c'\to\bar{p}p)\times B(\eta_c'\to\gamma\gamma) &\leq 7.0\times 10^{-8}, \text{ for assumed } \Gamma(\eta_c') = 10 \text{ MeV,} \end{aligned} \tag{8.34}$$

for η_c' with a mass anywhere in the range 3584 to 3624 MeV. The upper limits for the branching fraction product for the full range are shown as a function of the assumed mass $M(\eta_c')$ and width $\Gamma(\eta_c')$ in Fig. 8.22.

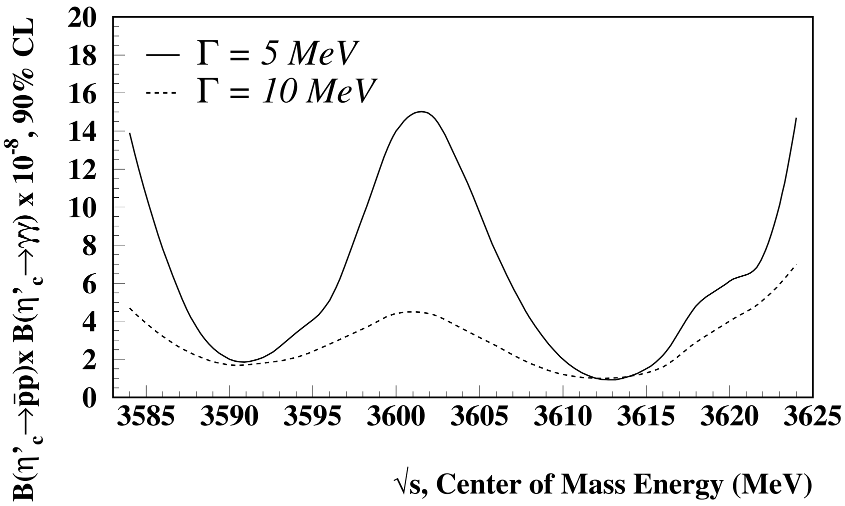

Figure 8.22: 90% CL upper limits for $B(\eta_c'\!\to\!\bar{p}p)\times B(\eta_c'\!\to\!\gamma\gamma)$ from E760, [50] for assumed $M(\eta_c')$ in the range 3584 to 3624 MeV, and assumed widths of $\Gamma(\eta_c')=5$ and 10 MeV.

The search for η_c' by E835

In experiment E835, we have searched for η_c' in a much wider mass region (3575 to 3660 MeV), with an investment of ~ 5 times greater luminosity, ~ 30 pb^{-1}. The spacing in $\sqrt{s}$ between data points was approximately 5 MeV. Despite this marathon effort, once again we have failed to find any evidence for η_c' production. The $\gamma\gamma$ cross sections measured in E835 for $|\cos\theta^*|\leq 0.4$ are presented in Fig. 8.23.

From these data we are only able to derive an upper limit for the branching fraction product $B(\eta_c'\!\to\!\bar{p}p)\times B(\eta_c'\!\to\!\gamma\gamma)$, for assumed values of the total width. The $\gamma\gamma$ cross sections for $|\cos\theta^*|\leq 0.4$ in the region $3576-3660$ MeV were fitted

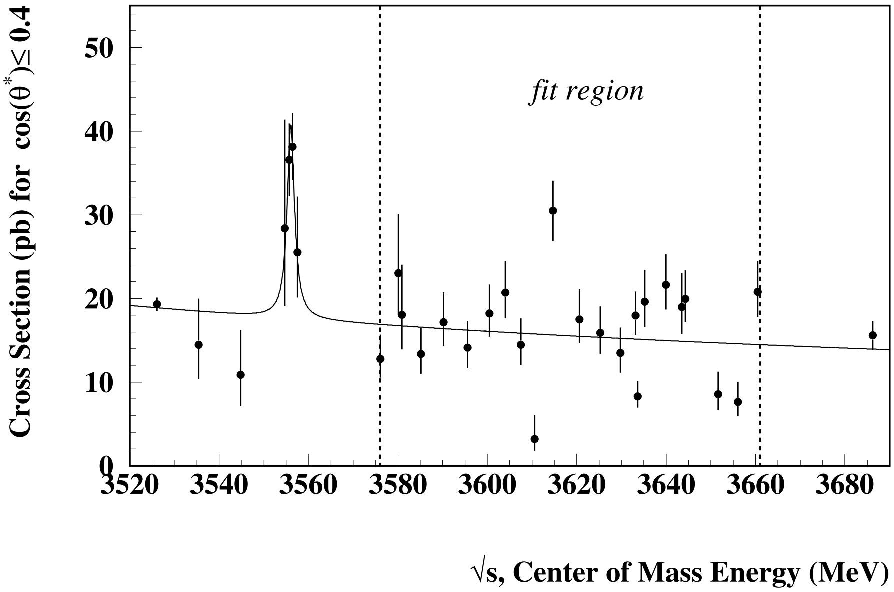

Figure 8.23: Measured cross sections for $\bar{p}p \rightarrow \gamma\gamma$ for $|\cos\theta^*| \leq 0.4$ in the η_c' search region. The χ_2 peak at $\sqrt{s} = 3556.18$ MeV is clearly visible.

for the branching fraction product, with various assumed fixed values of the η_c' mass and total width, (10, 15 and 20 MeV) and with the background parameters fixed to the values in Eq.8.22. The assumed mass of η_c' was varied in steps of 1 MeV from 3575 to 3660 MeV, and a maximum log likelihood fit was performed at each step. (see Appendix D).

The results of the fits are shown in Fig. 8.24. The summary of our results is that for η_c' masses between 3575 and 3660 MeV, the following 90% confidence upper limits can be set:

$$B(\eta_c' \rightarrow \bar{p}p) \times B(\eta_c' \rightarrow \gamma\gamma) \quad \leq 5.9 \times 10^{-8}, \text{ for } \Gamma(\eta_c') = 10 \text{ MeV, and}$$

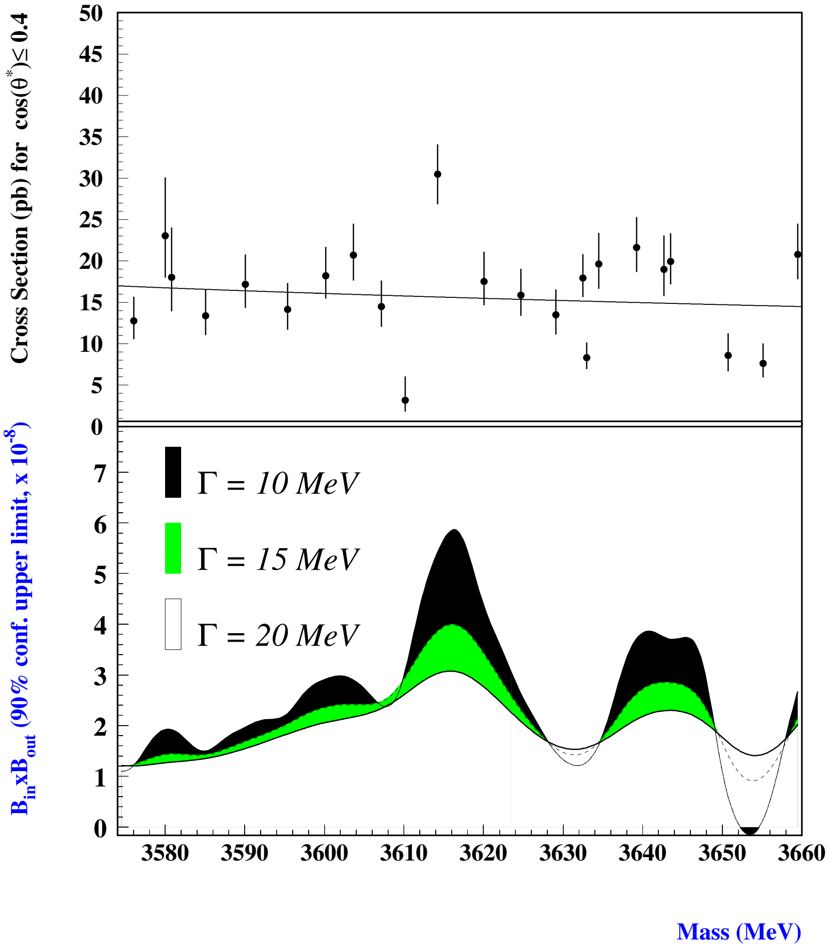

Figure 8.24: (Top) Measured cross sections for $\bar{p}p \to \gamma\gamma$ for $|\cos\theta^*| \leq 0.4$ in the η_c' search region. (Bottom) Result of maximum likelihood fits to these data. The three curves represent calculations of the 90% confidence upper limits on $B(\eta_c' \to \bar{p}p) \times B(\eta_c' \to \gamma\gamma)$ for assumed values of $\Gamma(\eta_c') = 10$, 15 and 20 MeV.

$$B(\eta_c'\to\bar{p}p)\times B(\eta_c'\to\gamma\gamma) \leq 4.0\times 10^{-8}, \text{ for } \Gamma(\eta_c') = 15 \text{ MeV, and}$$

$$B(\eta_c'\to\bar{p}p)\times B(\eta_c'\to\gamma\gamma) \leq 3.1\times 10^{-8}, \text{ for } \Gamma(\eta_c') = 20 \text{ MeV.} \tag{8.35}$$

The largest of these limits is more than a factor 4 smaller than the corresponding result for η_c, $B(\eta_c\to\bar{p}p)\times B(\eta_c\to\gamma\gamma) = 25.3^{+4.6}_{-4.5}\times 10^{-8}$.

Comments on η_c'

We wish to examine the above results in terms of the theoretical and phenomenological expectations.

Estimates of $B(\eta_c'\to\gamma\gamma)$

The ratio of the lowest order predictions for the $\gamma\gamma$ and gg partial widths of any state of charmonium is independent of the radial quantum number. From Table 2.1, for both η_c and η_c',

$$\Gamma(^1S_0\to gg) = \frac{8\pi{\alpha_{\rm S}}^2}{3m_c^2}|\psi_S(0)|^2(1+4.8\alpha_{\rm S}/\pi) \tag{8.36}$$

$$\Gamma(^1S_0\to\gamma\gamma) = \frac{64\pi{\alpha_{\rm EM}}^2}{27m_c^2}|\psi_S(0)|^2(1-3.4\alpha_{\rm S}/\pi) \tag{8.37}$$

Thus,

$$\frac{\Gamma(^1S_0\to\gamma\gamma)}{\Gamma(^1S_0\to gg)} = B(^1S_0\to\gamma\gamma) = \frac{8{\alpha_{\rm EM}}^2}{9{\alpha_{\rm S}}^2}\times\frac{(1-3.4\alpha_{\rm S}/\pi)}{(1+4.8\alpha_{\rm S}/\pi)}, \tag{8.38}$$

since we have established that both η_c and η_c' have total widths which are essentially completely hadronic. Therefore, we expect that

$$B(\eta_c'\to\gamma\gamma)\sim B(\eta_c\to\gamma\gamma) = (2.1\times 10^{-4}). \tag{8.39}$$

Estimates of $B(\eta_c'\to\bar{p}p)$

The prediction for the branching fraction $B(\eta_c'\to\bar{p}p)$ is somewhat less straightforward. We may assume that the ratio of $\Gamma(c\bar{c}\to\bar{p}p)/\Gamma(c\bar{c}\to hadrons)$ between radial excitations of the triplet states (J/ψ and ψ') is the same as that between the radial excitations of the singlet states (η_c and η_c'). *i.e.*,

$$\frac{\Gamma(\eta_c'\to\bar{p}p)/\Gamma(\eta_c'\to hadrons)}{\Gamma(\eta_c\to\bar{p}p)/\Gamma(\eta_c\to hadrons)} = \frac{\Gamma(\psi'\to\bar{p}p)/\Gamma(\psi'\to hadrons)}{\Gamma(J/\psi\to\bar{p}p)/\Gamma(J/\psi\to hadrons)} \tag{8.40}$$

$$\therefore B(\eta_c'\to\bar{p}p) = B(\eta_c\to\bar{p}p) \times \frac{\Gamma(\psi'\to\bar{p}p)/\Gamma(\psi'\to hadrons)}{\Gamma(J/\psi\to\bar{p}p)/\Gamma(J/\psi\to hadrons)} \tag{8.41}$$

$$\begin{aligned}\therefore B(\eta_c'\to\bar{p}p) \times 10^4 &= (12\pm 4)\frac{(0.19\pm 0.05\times 10^{-3})/(15.18\pm 3.36\times 10^{-2})}{(2.14\pm 0.10\times 10^{-3})/(70.7\pm 0.6\times 10^{-2})} \\ &= (12\pm 4)\times(0.413\pm 0.143) \\ &= 4.9\pm 2.4. \end{aligned} \tag{8.42}$$

Combining this with Eq. 8.40, we obtain

$$B(\eta_c'\to\bar{p}p) \times B(\eta_c'\to\gamma\gamma) \approx 10.3\pm 5.0\times 10^{-8}. \tag{8.43}$$

Thus the experimental limits which we have established in Eq. 8.36 are consistent with these semi-phenomenological expectations.

<u>Recent results from DELPHI</u>

Earlier, (Sec. 8.3.3) we mentioned $\Gamma_{\gamma\gamma}$ obtained for η_c and χ_2 resonances by photon-photon fusion experiments. It is worthwhile to look into what these experiments have to say about $\Gamma_{\gamma\gamma}(\eta_c')$. Actually, only one measurement has been reported so far. The DELPHI collaboration at LEP has recently published a result [98] which may add an alternate perspective on the question of our non-observation of η_c' in the reaction $\bar{p}p\to\eta_c'\to\gamma\gamma$. The usual expectation for the partial width $\Gamma(\eta_c'\to\gamma\gamma)$ is that

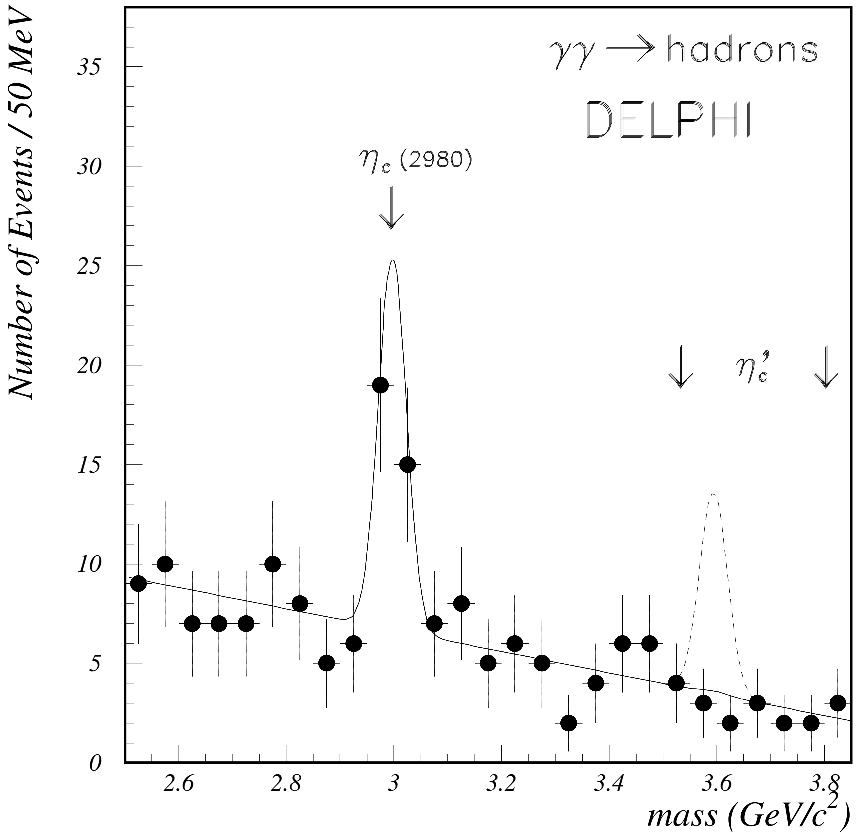

Figure 8.25: The sum of invariant mass distributions from DELPHI for five hadronic channels. The solid curve shows the result of a fit using two Gaussian functions for η_c and η_c', and a linear background. The dashed curve shows the expected signal for η_c' production, assuming $B(\eta_c' \rightarrow\ hadrons) = B(\eta_c \rightarrow\ hadrons)$ and that $\Gamma(\eta_c' \rightarrow \gamma\gamma) = 0.75\Gamma(\eta_c \rightarrow \gamma\gamma)$. This figure is taken from Ref. [98].

it is $|\psi_{2S}(0)|^2/|\psi(0)_{1S}|^2 \times \Gamma(\eta_c \to \gamma\gamma) = 0.6 \times \Gamma(\eta_c \to \gamma\gamma)$. (See Eq. 8.38) However, DELPHI has obtained a result which suggests that this might not be the case.

In their $\gamma\gamma$ fusion measurements, DELPHI clearly observes η_c in several hadronic decay channels. In Fig. 8.25 we show the sum of invariant mass distributions from five hadronic channels from DELPHI. The dashed curve in the figure shows the expected signal of η_c' production assuming the prediction of $\Gamma(\eta_c' \to \gamma\gamma)/\Gamma(\eta_c \to \gamma\gamma) = 0.75$ by Barnes [99]. A 90% confidence upper limit was set by DELPHI for the ratio of $\gamma\gamma$ partial widths,

$$\frac{\Gamma(\eta_c' \to \gamma\gamma)}{\Gamma(\eta_c \to \gamma\gamma)} \leq 0.34, \quad 90\% \text{ CL.} \tag{8.44}$$

Preliminary results from L3 suggest that a much lower limit may be set soon. [90]

8.7 Summary of Results

A summary of our results for the resonance parameters of η_c and χ_2, and limits we have set for χ_0 and η_c' is presented in Table 8.9.

8.8 Discussion of Results

In this section we summarize recently published theoretical predictions for the $\gamma\gamma$ and gg partial widths of the four charmonium states, η_c, η_c', χ_0 and χ_2. The predictions presented in this section are of two varieties - those that attempt a relativistic treatment of the bound state decays to the lowest order in α_s, and those which are essentially non-relativistic, but which go to higher orders in α_s. Predictions for the

Table 8.9: Summary of results presented in this dissertation.

$M(\eta_c)$	$2982.4^{+2.3}_{-2.2}$ MeV
$\Gamma(\eta_c)$	$26.9^{+10.8}_{-9.5}$ MeV
$\Gamma(\eta_c \to \gamma\gamma)$	$5.7^{+2.9+2.9}_{-2.3-1.4}$ keV
$\Gamma(\chi_2 \to \gamma\gamma)$	$0.343^{+0.053+0.043}_{-0.051-0.038}$ keV
90% confidence upper limits	
$\Gamma(\chi_0 \to \gamma\gamma)$	1.3 keV
$B(\eta_c' \to \bar{p}p) \times B(\eta_c' \to \gamma\gamma)$ for $\Gamma(\eta_c') = 10 - 20$ MeV	6×10^{-8}

η_c and η_c' partial widths are shown in Table 8.10. Predictions for χ_0 and χ_2 are shown in Table 8.11.

Table 8.10: Theoretical predictions for $\gamma\gamma$ and gg partial widths of η_c and η_c'. Assumed values for m_c and α_S are indicated where applicable. None of these predictions employ radiative corrections. We also present here our measurements of these partial widths. (GI = Godfrey and Isgur, AB = Ackleh and Barnes, GJR = Gupta, Johnson and Repko, and LS = Linde and Snellmann)

Authors	Ref.	m_c (GeV)	α_{S}	$\Gamma(\eta_c \to \gamma\gamma)$ (keV)	$\Gamma(\eta_c' \to \gamma\gamma)$ (keV)	$\Gamma(\eta_c \to gg)$ (MeV)	$\Gamma(\eta_c' \to gg)$ (MeV)
GI	[91]	1.63	0.34	6.76	4.84	22.09	7.29
AB	[92]	1.4	0.4	4.8	3.7	-	-
GJR	[94]	2.09	0.316	10.94	-	23.03	-
LS	[93]	1.276-1.366	0.211-0.277	6.2-6.5	-	-	-
E835		–	–	$5.7^{+2.9+2.9}_{-2.3-1.4}$	–	$26.9^{+10.8}_{-9.5}$	–

Table 8.11: Theoretical predictions for $\gamma\gamma$ and gg partial widths of χ_0 and χ_2. Assumed values for m_c and α_S are indicated where applicable. We also present here our measurements of these partial widths. (BBL = Bodwin, Braaten and Lepage, GJR = Gupta, Johnson and Repko, LS = Linde and Snellmann, HQC = Huang, Qiao and Chao, and HC = Huang and Chao)

Authors	Ref.	m_c (GeV)	$\alpha_{\rm s}$	$\Gamma(\chi_2 \to \gamma\gamma)$ (keV)	$\Gamma(\chi_0 \to \gamma\gamma)$ (keV)	$\Gamma(\chi_2 \to gg)$ (MeV)	$\Gamma(\chi_0 \to gg)$ (MeV)
^{a}BBL	[96]	-	0.25	0.81 ± 0.22	3.3 ± 0.9	1.71^*	4.7 ± 0.7
^{a}GJR	[94]	2.088	0.316	0.57	6.38	1.20	13.44
^{a}LS	[93]	1.28-1.37	0.21-0.28	0.31-0.41	1.5-1.8	-	-
^{b}HQC	[95]	1.4-1.6	0.29	0.39-0.50	4.85-5.82	-	-
^{b}HC	[97]	-	0.29	0.49 ± 0.15	3.72 ± 1.11	1.71^*	12.6 ± 3.2
E835		–	–	$0.343^{+0.053+0.043}_{-0.051-0.038}$	≤ 1.3(90% CL)	$1.71 \pm 0.16^\dagger$	$16.7^{+5.2}_{-3.7} \pm 0.1$

^{a} Used no radiative corrections

^{b} Used radiative corrections

* Input value

† Derived from E760's measurement of $\Gamma(\chi_2) = 1.98 \pm 0.18$ MeV, and the PDG value $B(\chi_2 \to \gamma J/\psi) = 0.135 \pm 0.011$.

Relativistic calculations

Several papers in the literature address theoretically the two-gluon and two-photon decays of charmonium states from a relativistic point of view. Much of this work was catalyzed by the first measurements of χ_1 and χ_2 total widths and branching ratios by E760.

Two calculations of the relativistic variety are given by Godfrey and Isgur (GI) [91] and Ackleh and Barnes (AB) [92]. GI calculated masses, electromagnetic decay widths, annihilation widths, etc., for "all mesons - from the pion to the upsilon" [91] in a single framework. AB calculated the two-photon decay widths of both light and heavy singlet quarkonia, modeled after a fully-relativistic treatment of singlet positronium.

Both GI and AB use wave functions calculated in a non-relativistic Coulomb+linear potential, and attempt to account for all relativistic corrections to annihilation amplitudes which have been calculated for a free quark-antiquark pair.

In Ref. [93], Linde and Snellmann present a relativistic calculation of $\gamma\gamma$, E1 and M1 decays of charmonium states. Their calculation is done using the Bethe-Salpeter formalism, and a potential with vector one-gluon exchange, and scalar confinement. They determine the parameters of their model by a fit to the charmonium mass spectrum and to the leptonic decay rate of J/ψ.

Gupta, Johnson and Repko (GJR) present $\gamma\gamma$ and two-gluon decay rates for charmonium states, [94] using their own "realistic" QCD-inspired potential. [84] GJR claim that they have calculated their transition widths in a fully-relativistic manner, including off-shell quarks. They also claim that their model treats the spin-dependent quark-antiquark interaction non-perturbatively. Their model has the rather unusual feature of predicting identical ratios $B((c\bar{c})_R \to \gamma\gamma)/B((c\bar{c})_R \to gg)$ for χ_0, χ_2 and η_c.

Huang, Qiao and Chao (HQC) present results from relativistic calculations in the Bethe-Salpeter formalism, and they include radiative corrections to NLO in α_s. [95] Their potential is a QCD-inspired phenomenological potential, with vector one gluon exchange, and scalar confinement.

Non-Relativistic QCD calculations

We present two NRQCD predictions which are based on the factorization formalism of Bodwin, Braaten and Lepage (hereafter, BBL) [96].

Early calculations of charmonium decays, including those presented in Ref. [23], attempt to deal with non-perturbative effects by factoring them into the wave function at the origin, $\psi(0)$, in the case of S-state charmonium, or into the derivative of the radial wave function at the origin, $R'(0)$, in the case of P-states. BBL noted [96] that this factorization assumption is not valid for P-states, since order $\alpha_s{}^3$ calculations revealed infrared divergences. The presence of those divergences indicated that not all non-perturbative effects could be factored into $R'(0)$.

BBL argued for the addition of another phenomenological parameter (aside from $R'(0)$), which was related to the probability that the c and $\bar{c}$ quarks in the charmonium could be found in a color octet state. By using measured decay rates of χ_2 and χ_1 to light hadrons, BBL present predictions for the light hadron decays of the other two P-states (χ_0 and ${}^1P_1$), as well as two-photon decays of χ_0 and χ_2, to lowest order in α_{s}. Huang and Chao [97] also use the BBL formalism, with corrections which are next-to-leading order in α_{s}.

All the partial width predictions assume values for the strong coupling constant $\alpha_{\mathrm{s}}(m_c)$ and/or for the charm quark mass m_c. The assumed values of these parameters are listed in the tables along with the width predictions.

Comparison of E835 results to the theoretical predictions

The predictions for $\Gamma(\eta_c \to \gamma\gamma)$ are the other predictions are generally in agreement with our result, $\Gamma(\eta_c \to \gamma\gamma) = 5.7^{+2.9+2.9}_{-2.3-1.4}$ keV. The sole exception is the high value, 10.94 keV, predicted by Gupta *et al.* , [94].

Both the predictions of $\Gamma(\eta_c \to gg)$ which we presented are surprisingly close to our experimental result of $\Gamma(\eta_c) = 26.9^{+12.1}_{-8.5}$ MeV. Interestingly, the prediction by Godfrey and Isgur predates the E760 measurement of $\Gamma(\eta_c) = 23.9^{+12.6}_{-7.1}$ MeV by about ten years.

The predictions for $\Gamma(\chi_2 \to \gamma\gamma)$ are generally in agreement with each other, and with our measured value, $\Gamma(\chi_2 \to \gamma\gamma) = 0.343^{+0.053+0.043}_{-0.051-0.038}$ keV. The predictions for $\Gamma(\chi_0 \to \gamma\gamma)$ are more variable, and are generally much larger than the 90% confidence upper limit, $\Gamma(\chi_0 \to \gamma\gamma) \leq 1.3$ keV, established by us.